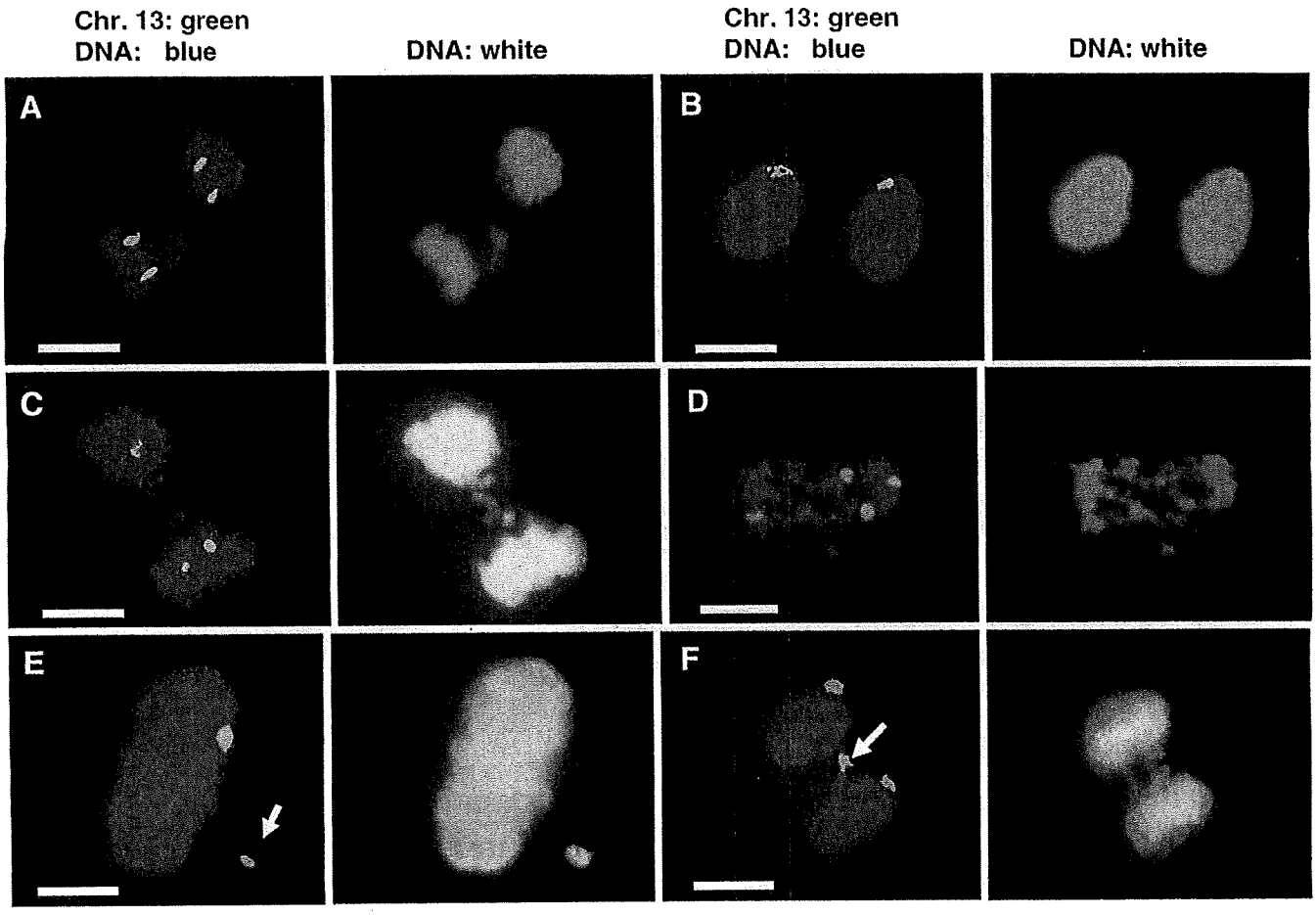

Figure 3. Segregation of chromosome 13 at anaphase or telophase. UE6E7T-3 cells were analyzed by FISH using chromosome 13-specific probes. All *left-hand panels* (*A–F*) show chromosome 13 (*green*) and DNA (*blue*); all *right-hand panels* show DNA (*white*). There was normal segregation of cells with (*A*) two copies or (*B*) one copy of chromosome 13. Abnormal segregation of cells in which the copies of chromosome 13 unequally segregate into daughter cells with (*C*) one and two copies or (*D*) three copies of the chromosome also occurred. Abnormal segregation of cells displaying one misaligned copy of chromosome 13 in a metaphase cell (*E*, *arrow*) and trapping of a lagging chromosome 13 in the anaphase bridge (*F*, *arrow*) are shown. *Scale bar*, 10 μm; *Chr* chromosome.

chromosome 13 (Fig. 4*Ba*) and may subsequently result in chromosome instability. We were especially interested in the observations that one of the two copies of chromosome 13 was lost non-randomly and that loss of chromosome 13 might occur via MSI. Specifically, three, two, four, and four bands were observed for each of the four PCR products obtained for the UE6E7T-3 cells with the microsatellite markers D13S1493, D13S153, D13S788, and D13S800, respectively (Fig. 4*B*). However, the PCR product for D13S154 was a single homologous band (data not shown). As shown in Fig. 2, one copy of chromosome 13 was observed for UE6E7T-3 cells at PDL118. Each PCR product obtained from this cell by using the microsatellite markers was one band (Fig. 4*Bb*). For the UE6E7T-3 cells at PDL101, LOH was also detected for chromosome 13 with any of the four markers (D13S1493, D13S153, D13S788, and D13S800) which were widely localized to chromosome 13.

In order to confirm non-random loss of chromosome 13, SNP analysis of chromosome 13 in UE6E7T-3 cells at PDL101 was accomplished using the Affymetrix Gene Chip Human Mapping 250K Nsp Array Set (Fig. 5). The total number of SNPs detected for the genome was 262,262 in UE6E7T-3 cells (at PDL78) which retained two copies of chromosome 13 (Fig. 5). Of the 11,117 SNPs on chromosome 13 in UE6E7T-3 cells (PDL 78), 10,586 SNPs were detected by the array kit. The call rate of SNPs analyzed on chromosome 13 was 95.2% in this assay. The number of heterozygous SNPs among the 11,117 SNPs on chromosome 13 in UE6E7T-3 cells at PDL78 was determined to be 2,359. These 2,359 SNPs were subsequently analyzed at PDL101 and 2,069 of the corresponding SNP sites (88%) were detected as homozygous sequences. These results show that specific one copy of chromosome 13 was lost non-randomly. A partial strand of chromosome 16 changed from heterozygous to homozygous, as shown in Fig. 5. In a

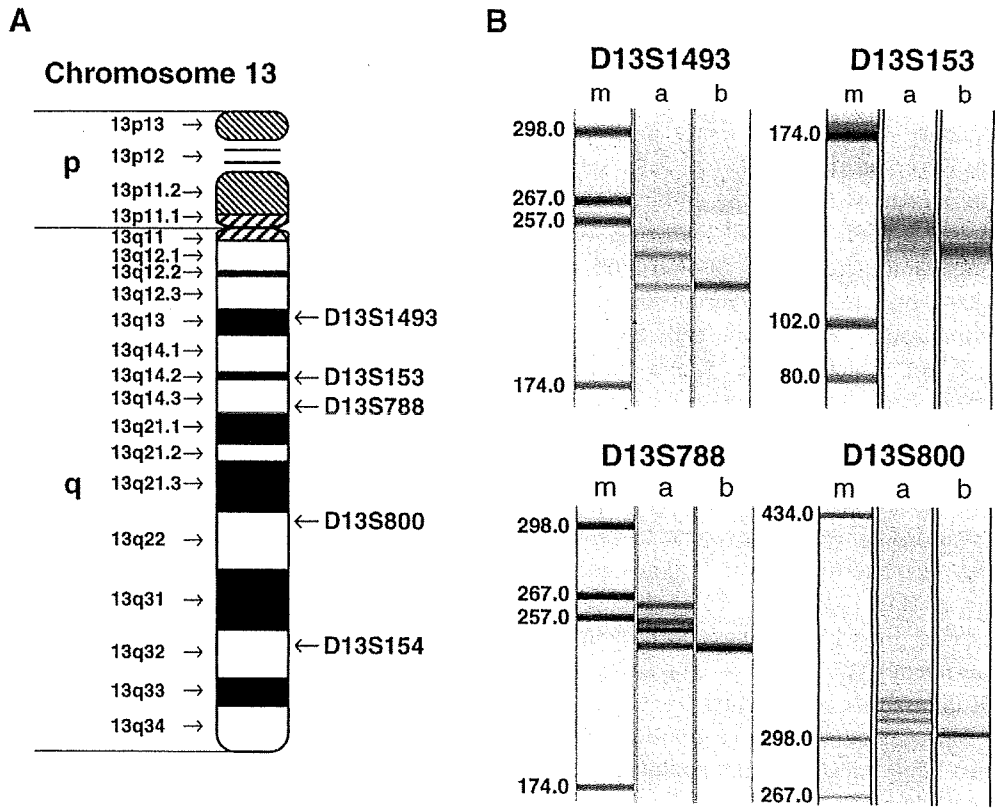

Figure 4. Microsatellite analysis of chromosome 13 in UE6E7T-3 cells. (*A*) Map of chromosome 13. The five microsatellite markers used in this study are indicated by *arrows* (*right*). (*B*) *Middle* and *right* column patterns in each microsatellite marker group show PCR products obtained from UE6E7T-3 cells at (*a*) PDL78 or (*b*) PDL147, respectively, with each of the four microsatellite primer sets shown in Table 1. *Ba*, PDL78 DNA. *Bb*, PDL147 DNA. *Bm* indicates molecular weight markers of DNA.

previous report (Takeuchi et al. 2007), loss of the q-arm of chromosome 16 was observed in UE6E7T-3 cells at PDL101 by array CGH analysis. This loss of chromosome 16 was due to a partial q-arm change. In this report, we did not further investigate the loss of chromosome 16 by microsatellite analysis.

Discussion

Here, we have presented data to show that the loss of one or two chromosomes in the UE6E7T-3 cell line directly caused near-diploid aneuploidy and that this occurred independently of tetraploid intermediates. Evidence for this

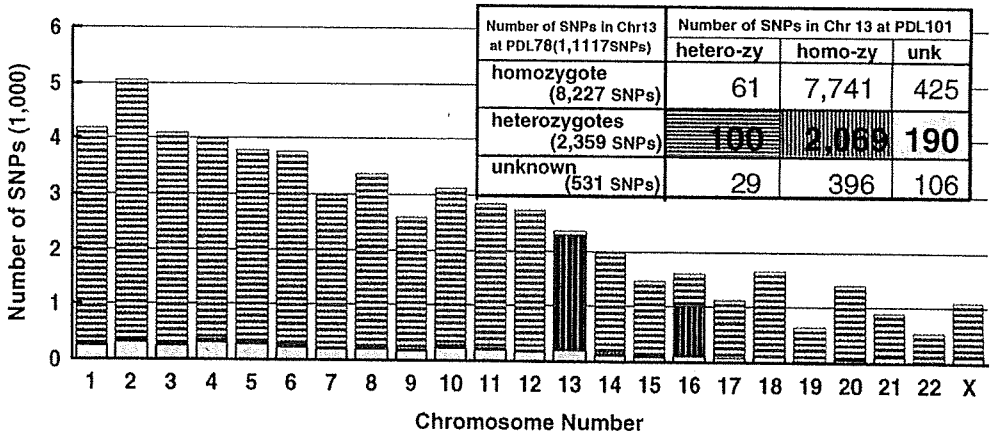

Figure 5. Heterozygosity of SNPs on chromosome 13 at PDL101 that correspond to those at PDL78. The total number of SNPs detected using the Affymetrix Gene Chip Human Mapping 250K Assay Set was 262,262 in whole genome at PDL78 for the UE6E7T-3 cells. There were 11,117 SNPs on chromosome 13 in the cell. The distribution of SNPs at PDL101 corresponded to 2,359 of the heterozygous SNPs at PDL78 was shown as homozygote (*vertical line*), heterozygote (*horizontal line*), or unknown (no call; *white*) SNPs. *SNP* single nucleotide polymorphism, *Chr* chromosome, *PDL* population doubling level, *hetero-zy* heterozygotes, *homo-zy* homozygotes, *unk* unknown.

includes the following: (1) At early stages of long-term culture (e.g., PDL85), the population of cells that contained 46 chromosomes decreased and a new population that contained 42–45 chromosomes appeared, but no tetraploidy was observed (Fig. 1). (2) At later stages (e.g., PDL118), approximately 70% of the cultured cells contained 42–45 chromosomes and had lost one or more copies of chromosome containing chromosome 13, and 18% of the cells contained 71–90 chromosomes with two copies of chromosome 13. However, cells that contained four copies were not detected (Figs. 1 and 2). (3) FISH images of chromosomes in metaphase or anaphase showed three patterns through which UE6E7T-3 cells lost a copy of chromosome 13. These were unequal segregation of chromosome 13 during mitosis (Fig. 3*C*, *D*), exclusion of the misaligned chromosome 13 on the metaphase plate (Fig. 3*E*), and trapping of chromosome 13 in the midbody region (Fig. 3*F*). The FISH images provide the first instance in which it has been possible to follow the movement of a specific chromosome, such as chromosome 13, throughout cell division.

Missegregation of the chromosomes during mitosis will most likely yield near-diploid aneuploidy. Several molecular mechanisms through which aneuploidy may be generated have been recently proposed, but the precise mechanism remains largely unclear. Many studies have suggested that aneuploidy arises from defects in the conserved spindle checkpoint in which a large number of gene products participate, including BUB1, BUBR1, BUB3, MAD1, MAD2, MPS, Aurora B, and CENP-E. It has been shown that decreased expression of one or more checkpoint components leads to near-diploidy, and that a complete inactivation of these checkpoint genes results in embryonic lethality. Weaver et al. (2003) reported that mouse fibroblasts with a heterogeneous CENP-E gene, induced by knockout of the mitosis-specific motor protein CENP-E, tended to gain or lose only one or two chromosomes, without inducing failed cytokinesis, resulting in near-diploid aneuploidy and promotion of tumorigenesis (Kops et al. 2005). Similarly, Mad2, BuBR1, or BuB3 haploinsufficient mice exhibit an impaired mitotic checkpoint response and develop near-diploid aneuploidy (Michel et al. 2001; Babu et al. 2003; van Deursen 2007). Our data cannot, however, be explained by near-diploid aneuploidy generated through decreased expression of the checkpoint proteins because chromosome loss occurred specifically for one copy of chromosome13 and not for just any chromosome as observed in the cases of reduced checkpoint proteins.

Overexpression of Mad2 or BuBR1 blocks an essential step in cell division and induces failure of cytokinesis, resulting in tetraploidization, and the formation of a wide variety of tumors (Sotillo et al. 2007). Recently, a challenging proposal was made that nondisjunction of chromosomes during mitosis does not produce near-diploid aneuploid cells directly, but instead gives rise to mitotic cleavage failure, resulting in tetraploidy. These tetraploid cells could subsequently become aneuploid through further cell division, being transient intermediates during tumorigenesis in human cell lines (Shi and King 2005). However, the mechanistic basis for the tetraploid formation still remains to be elucidated. In this study, we also observed tetraploid UE6E7T-3 cells at late PDLs, but these cells most likely arose from the fusion of near-diploid cells after the loss of one copy of chromosome 13, because two copies, not four, were observed in the tetraploid cells (Fig. 2*A*).

Missegregation can also occur as a consequence of the inappropriate attachment of microtubules to spindle poles, as a monotelic attachment. The lagging of one copy of chromosome 13 might be produced by such a mechanism, resulting in its exclusion from daughter cells (Fig. 3*E*, *F*). The microsatellite analysis of chromosome 13 suggests that the structural mutation of microsatellite DNA leads to the mutation of essential loci on chromosome 13 for microtubule attachment. At early culture stage, UE6E7T-3 cells had a normal karyotype in which a copy of chromosome 13 contained various microsatellites different from the corresponding allele at four loci (microsatellite instability), and lost the chromosome 13 with these microsatellites in prolonged culture, indicating LOH (Fig. 4*B*). In addition, whole genome SNP assay with nearly 262,000 SNP markers confirmed the non-random loss of chromosome 13 (Fig. 5).

Loss of a copy of chromosome 13 has also been frequently reported in human endothelial cells from umbilical cord veins (Zhang et al. 2000; Kimura et al. 2004; Anno et al. 2007) and bone marrow (Wen et al. 2006). A number of studies have showed that LOH on chromosome 13 is a common feature of malignancies such as retinoblastoma and breast tumors, arising after the loss of the remaining normal allele in heterozygotes (Hagstrom and Dryja 1999; Berwick et al. 2007). LOH on chromosome 13 has also been observed in normal human vascular endothelial cells in culture (Kimura et al. 2004), but the mechanism as to why only one copy of chromosome 13 is lost remains unknown. In light of the current results, it is possible that MSI may play an important role in the loss of chromosome 13 in the UE6E7T-3 cell line.

MSI is caused by a failure of the DNA mismatch repair system to repair errors that occur during DNA replication and is characterized by the accelerated accumulation of single nucleotide mutations and alteration in the length of simple, microsatellite sequences (Miturski et al. 2002). If a strand-alignment error remains unrepaired, it will result in a frameshift mutation, leading to adjacent DNA sequence error(s) including centromere and coding regions. Centro-

meres serve both as the sites of association of sister chromatids and as attachment sites for microtubules of the mitotic spindle. They consist of specific DNA sequences to which a number of centromere association proteins bind, forming a special structure called the kinetochore. Taken together with our results, these findings suggests that the loss of a single chromosome 13 with MSI probably occurs by mutation of essential centromere DNA-containing microtubule attachment sites and does not involve the mutation of the known tumor suppressor gene (RB1) on chromosome 13.

In conclusion, we showed by FISH with a probe specific for chromosome 13, that the preferential loss of chromosome 13 in UE6E7T-3 cell line is caused by chromosome missegregation, which results directly in near-diploid aneuploidy. In addition, microsatellite and SNP analyses showed non-random loss of a single copy of chromosome 13 that had MSIs at four loci. This finding suggests the mutation of essential loci on chromosome 13 for microtubule attachment. Thus, the results may contribute significantly to a better understanding of how aneuploid cells arise and help to elucidate the mechanisms of chromosomal instability in carcinogenic progression and in the non-random loss of chromosomes.

Acknowledgements This study was supported in part by a grant from the Ministry of Health, Labor, and Welfare of Japan. We are very grateful to all members of The Cell Bank (JCRB and HSRRB) for assistance and discussion. M.T. and K.T. contributed equally to this work.

References

Anno, K.; Hayashi, A.; Takahashi, T.; Mitsui, Y.; Ide, T.; Tahara, H. Telomerase activation induces elongation of the telomeric single-stranded overhang, but does not prevent chromosome aberrations in human vascular endothelial cells. *Biochem. Biophys. Res. Commun.* 353: 926–932; 2007 doi:10.1016/j.bbrc.2006.12.112.

Babu, J. R.; Jeganathan, K. B.; Baker, D. J.; Wu, X.; Kang-Decker, N.; van Deursen, J. M. Rael is an essential mitotic checkpoint regulator that cooperates with Bub3 to prevent chromosome missegregation. *J. Cell Biol.* 160: 341–353; 2003 doi:10.1083/jcb.200211048.

Berwick, M.; Satagopan, J. M.; Ben-Porat, L.; Carlson, A.; Mah, K.; Henry, R.; Diotti, R.; Milton, K.; Pujara, K.; Landers, T.; Dev, B. S.; Morales, J.; Schindler, D.; Hanenberg, H.; Hromas, R.; Levran, O.; Auerbach, A. D. Genetic heterogeneity among Fanconi anemia heterozygotes and risk of cancer. *Cancer Res.* 67: 9591–9596; 2007 doi:10.1158/0008-5472.CAN-07-1501.

Bharadwaj, R.; Yu, H. The spindle checkpoint, aneuploidy, and cancer. *Oncogene* 23: 2016–2027; 2004 doi:10.1038/sj.onc.1207374.

Dobles, M.; Liberal, V.; Scott, M. L.; Benezra, R.; Sorger, P. K. Chromosome missegregation and apoptosis in mice lacking the mitotic checkpoint protein Mad2. *Cell* 101: 635–645; 2000 doi:10.1016/S0092-8674(00)80875-2.

Galipeau, P. C.; Cowan, D. S.; Sanchez, C. A.; Barrett, M. T.; Emond, M. J.; Levine, D. S.; Rabinovitch, P. S.; Reid, B. J. 17p (p53) allelic losses, 4N (G2/tetraploid) populations, and progression to aneuploidy in Barrett's esophagus. *Proc. Natl. Acad. Sci. U. S. A.* 93: 7081–7084; 1996 doi:10.1073/pnas.93.14.7081.

Hagstrom, S. A.; Dryja, T. P. Mitotic recombination map of 13cen-13q14 derived from an investigation of loss of heterozygosity in retinoblastomas. *Proc. Natl. Acad. Sci. U. S. A.* 96: 2952–2957; 1999 doi:10.1073/pnas.96.6.2952.

Hanks, S.; Coleman, K.; Reid, S.; Plaja, A.; Firth, H.; Fitzpatrick, D.; Kidd, A.; Mehes, K.; Nash, R.; Robin, N.; Shannon, N.; Tolmie, J.; Swansbury, J.; Irrthum, A.; Douglas, J.; Rahman, N. Constitutional aneuploidy and cancer predisposition caused by biallelic mutations in BUB1B. *Nat. Genet.* 36: 1159–1161; 2004 doi:10.1038/ng1449.

Ionov, Y.; Peinado, M. A.; Malkhosyan, S.; Shibata, D.; Perucho, M. Ubiquitous somatic mutations in simple repeated sequences reveal a new mechanism for colonic carcinogenesis. *Nature* 363: 558–561; 1993 doi:10.1038/363558a0.

Kimura, M.; Cao, X.; Patel, S.; Aviv, A. Survival advantage of cultured human vascular endothelial cells that lost chromosome 13. *Chromosoma* 112: 317–322; 2004 doi:10.1007/s00412-004-0276-6.

Kops, G. J.; Foltz, D. R.; Cleveland, D. W. Lethality to human cancer cells through massive chromosome loss by inhibition of the mitotic checkpoint. *Proc. Natl. Acad. Sci. U. S. A.* 101: 8699–8704; 2004 doi:10.1073/pnas.0401142101.

Kops, G. J.; Weaver, B. A.; Cleveland, D. W. On the road to cancer: aneuploidy and the mitotic checkpoint. *Nat. Rev. Cancer* 5: 773–785; 2005 doi:10.1038/nrc1714.

Lengauer, C.; Kinzler, K. W.; Vogelstein, B. Genetic instability in colorectal cancers. *Nature* 386: 623–627; 1997 doi:10.1038/386623a0.

Lindblad-Toh, K.; Tanenbaum, D. M.; Daly, M. J.; Winchester, E.; Lui, W. O.; Villapakkam, A.; Stanton, S. E.; Larsson, C.; Hudson, T. J.; Johnson, B. E.; Lander, E. S.; Meyerson, M. Loss-of-heterozygosity analysis of small-cell lung carcinomas using single-nucleotide polymorphism arrays. *Nat. Biotechnol.* 18: 1001–1005; 2000 doi:10.1038/79269.

Meraldi, P.; Draviam, V. M.; Sorger, P. K. Timing and checkpoints in the regulation of mitotic progression. *Dev. Cell* 7: 45–60; 2004 doi:10.1016/j.devcel.2004.06.006.

Michel, L.; Diaz-Rodriguez, E.; Narayan, G.; Hernando, E.; Murty, V. V.; Benezra, R. Complete loss of the tumor suppressor MAD2 causes premature cyclin B degradation and mitotic failure in human somatic cells. *Proc. Natl. Acad. Sci. U. S. A.* 101: 4459–4464; 2004 doi:10.1073/pnas.0306069101.

Michel, L. S.; Liberal, V.; Chatterjee, A.; Kirchwegger, R.; Pasche, B.; Gerald, W.; Dobles, M.; Sorger, P. K.; Murty, V. V.; Benezra, R. MAD2 haplo-insufficiency causes premature anaphase and chromosome instability in mammalian cells. *Nature* 409: 355–359; 2001 doi:10.1038/35053094.

Miturski, R.; Bogusiewicz, M.; Ciotta, C.; Bignami, M.; Gogacz, M.; Burnouf, D. Mismatch repair genes and microsatellite instability as molecular markers for gynecological cancer detection. *Exp. Biol. Med. (Maywood.)* 227: 579–586; 2002.

Nigg, E. A. Centrosome aberrations: cause or consequence of cancer progression? *Nat. Rev. Cancer* 2: 815–825; 2002 doi:10.1038/nrc924.

Olaharski, A. J.; Sotelo, R.; Solorza-Luna, G.; Gonsebatt, M. E.; Guzman, P.; Mohar, A.; Eastmond, D. A. Tetraploidy and chromosomal instability are early events during cervical carcinogenesis. *Carcinogenesis* 27: 337–343; 2006 doi:10.1093/carcin/bgi218.

Pellman, D. Cell biology: aneuploidy and cancer. *Nature* 446: 38–39; 2007 doi:10.1038/446038a.

Pfeifer, D.; Pantic, M.; Skatulla, I.; Rawluk, J.; Kreutz, C.; Martens, U. M.; Fisch, P.; Timmer, J.; Veelken, H. Genome-wide analysis of DNA copy number changes and LOH in CLL using high-

density SNP arrays. *Blood* 109: 1202–1210; 2007 doi:10.1182/blood-2006-07-034256.

Piel, M.; Nordberg, J.; Euteneuer, U.; Bornens, M. Centrosome-dependent exit of cytokinesis in animal cells. *Science* 291: 1550–1553; 2001 doi:10.1126/science.1057330.

Powierska-Czarny, J.; Miscicka-Sliwka, D.; Czarny, J.; Grzybowski, T.; Wozniak, M.; Drewa, G.; Czechowicz, W.; Sir, J. Analysis of microsatellite instability and loss of heterozygosity in breast cancer with the use of a well characterized multiplex system. *Acta. Biochim. Pol.* 50: 1195–1203; 2003.

Putkey, F. R.; Cramer, T.; Morphew, M. K.; Silk, A. D.; Johnson, R. S.; McIntosh, J. R.; Cleveland, D. W. Unstable kinetochore-microtubule capture and chromosomal instability following deletion of CENP-E. *Dev. Cell* 3: 351–365; 2002 doi:10.1016/S1534-5807(02)00255-1.

Shi, Q.; King, R. W. Chromosome nondisjunction yields tetraploid rather than aneuploid cells in human cell lines. *Nature* 437: 1038–1042; 2005 doi:10.1038/nature03958.

Sotillo, R.; Hernando, E.; Diaz-Rodriguez, E.; Teruya-Feldstein, J.; Cordon-Cardo, C.; Lowe, S. W.; Benezra, R. Mad2 overexpression promotes aneuploidy and tumorigenesis in mice. *Cancer Cell* 11: 9–23; 2007 doi:10.1016/j.ccr.2006.10.019.

Takeuchi, M.; Takeuchi, K.; Kohara, A.; Satoh, M.; Shioda, S.; Ozawa, Y.; Ohtani, A.; Morita, K.; Hirano, T.; Terai, M.; Umezawa, A.; Mizusawa, H. Chromosomal instability in human mesenchymal stem cells immortalized with human papilloma virus E6, E7, and hTERT genes. *In Vitro Cell Dev. Biol. Anim.* 43: 129–138; 2007 doi:10.1007/s11626-007-9021-9.

van Deursen, J. M. Rb loss causes cancer by driving mitosis mad. *Cancer Cell* 11: 1–3; 2007 doi:10.1016/j.ccr.2006.12.006.

Weaver, B. A.; Bonday, Z. Q.; Putkey, F. R.; Kops, G. J.; Silk, A. D.; Cleveland, D. W. Centromere-associated protein-E is essential for the mammalian mitotic checkpoint to prevent aneuploidy due to single chromosome loss. *J. Cell Biol.* 162: 551–563; 2003 doi:10.1083/jcb.200303167.

Weaver, B. A.; Cleveland, D. W. Does aneuploidy cause cancer? *Curr. Opin. Cell Biol.* 18: 658–667; 2006 doi:10.1016/j.ceb.2006.10.002.

Weaver, B. A.; Silk, A. D.; Cleveland, D. W. Cell biology: nondisjunction, aneuploidy and tetraploidy. *Nature* 442: E9–10; 2006 doi:10.1038/nature05139.

Wen, V. W.; Wu, K.; Baksh, S.; Hinshelwood, R. A.; Lock, R. B.; Clark, S. J.; Moore, M. A.; Mackenzie, K. L. Telomere-driven karyotypic complexity concurs with p16INK4a inactivation in TP53-competent immortal endothelial cells. *Cancer Res.* 66: 10691–10700; 2006 doi:10.1158/0008-5472.CAN-06-0979.

Zhang, L.; Aviv, H.; Gardner, J. P.; Okuda, K.; Patel, S.; Kimura, M.; Bardeguez, A.; Aviv, A. Loss of chromosome 13 in cultured human vascular endothelial cells. *Exp. Cell Res.* 260: 357–364; 2000 doi:10.1006/excr.2000.4997.

Zheng, L.; Flesken-Nikitin, A.; Chen, P. L.; Lee, W. H. Deficiency of retinoblastoma gene in mouse embryonic stem cells leads to genetic instability. *Cancer Res.* 62: 2498–2502; 2002.

UICC
global cancer control

IJC
International Journal of Cancer

Check your cultures! A list of cross-contaminated or misidentified cell lines

Amanda Capes-Davis[1], George Theodosopoulos[1], Isobel Atkin[2], Hans G. Drexler[3], Arihiro Kohara[4], Roderick A.F. MacLeod[3], John R. Masters[5], Yukio Nakamura[6], Yvonne A. Reid[7], Roger R. Reddel[1] and R. Ian Freshney[8]

[1] CellBank Australia – Children's Medical Research Institute, Westmead, NSW, Australia
[2] European Collection of Cell Cultures (ECACC) – Health Protection Agency, Porton Down, Salisbury, Wiltshire, United Kingdom
[3] DSMZ – German Collection of Microorganisms and Cell Cultures, Braunschweig, Germany
[4] JCRB – Japanese Collection of Research Bioresources, Osaka, Japan
[5] Institute of Urology, University College London, London, United Kingdom
[6] RIKEN – BioResource Center Cell Engineering Division, Tsukuba, Japan
[7] ATCC – American Type Culture Collections, Manassas, VA
[8] Centre for Oncology and Applied Pharmacology, Glasgow University, Glasgow, United Kingdom

Mini Review

Continuous cell lines consist of cultured cells derived from a specific donor and tissue of origin that have acquired the ability to proliferate indefinitely. These cell lines are well-recognized models for the study of health and disease, particularly for cancer. However, there are cautions to be aware of when using continuous cell lines, including the possibility of contamination, in which a foreign cell line or microorganism is introduced without the handler's knowledge. Cross-contamination, in which the contaminant is another cell line, was first recognized in the 1950s but, disturbingly, remains a serious issue today. Many cell lines become cross-contaminated early, so that subsequent experimental work has been performed only on the contaminant, masquerading under a different name. What can be done in response—how can a researcher know if their own cell lines are cross-contaminated? Two practical responses are suggested here. First, it is important to check the literature, looking for previous work on cross-contamination. Some reports may be difficult to find and to make these more accessible, we have compiled a list of known cross-contaminated cell lines. The list currently contains 360 cell lines, drawn from 68 references. Most contaminants arise within the same species, with HeLa still the most frequently encountered (29%, 106/360) among human cell lines, but interspecies contaminants account for a small but substantial minority of cases (9%, 33/360). Second, even if there are no previous publications on cross-contamination for that cell line, it is essential to check the sample itself by performing authentication testing.

Key words: authentication, cell culture, cell lines, cross-contamination, DNA profiling, misidentification
Additional Supporting Information may be found in the online version of this article.
Novelty and Impact: This manuscript reviews the literature relating to cross-contamination of cell lines. Its novelty comes from the inclusion of a list of known cross-contaminated cell lines (over 300 lines named), allowing researchers to check their own cell lines with reference to the article. Recent developments in this field, including methods of authentication testing, are also discussed.
Grant sponsor: National Health and Medical Research Council of Australia
DOI: 10.1002/ijc.25242
History: Received 24 Nov 2009; Accepted 18 Jan 2010; Online 8 Feb 2010
Correspondence to: Amanda Capes-Davis, CellBank Australia, Children's Medical Research Institute, Locked Bag 23, Wentworthville, NSW 2145, Australia, Fax: +61 2 9687 2120, E-mail: acapdav@gmail.com

Cell Lines as Model Systems

Continuous cell lines represent a readily accessible and easily studied resource for research into health and disease. These cell lines have acquired the ability to proliferate indefinitely if grown in the appropriate culture conditions; usually this is a rare event, since the majority of cells even in tumor tissue will cease proliferation after a limited number of cell divisions.[1] However, once established, a continuous cell line can be repeatedly passaged, reliably recovers from cryopreservation and retains many of the properties of its cell type or tissue of origin.[2,3] These advantages make continuous cell lines effective, and widely used, model systems for normal cellular processes and for a variety of disease states.

Cell lines are particularly attractive models for studying malignant disease. The genetic changes in tumor-derived cell lines closely resemble those of the tumors of origin.[4] Moreover, the genetic changes required to establish continuous cell lines from normal cells recapitulate many of the genetic changes occurring in cancer.[5,6] These genetic changes are required to overcome replicative senescence, in which normal cells continue to be metabolically active but are restricted from further division.[1] Cells able to overcome senescence continue

proliferating until their telomeres become so short that the chromosomes undergo fusion-breakage-bridge cycles and the ensuing genomic instability results in culture crisis. Occasionally (at a rate of ~1 in 10^7 cells), an immortalized cell will emerge from crisis and begin to divide again, yielding a continuous cell line.[1] The changes seen throughout this process have many parallels within cancer development, both for malignancy in general and when considering specific tumor types.[7,8]

Despite these advantages, numerous cautions have emerged from the literature regarding appropriate use of cell lines as model systems.[9,10] Even where cultures have been transformed through the introduction of specific genes, cell lines that have passed through replicative senescence and crisis are aneuploid, heteroploid and genotypically and phenotypically unstable, resulting in considerable heterogeneity within the culture.[10] This instability will cause changes in the characteristics of the cell line but a further consequence may result: alterations in a cell line can be accepted by the user as intrinsic to that culture when there is actually extrinsic contamination present.

Cell Line Cross-contamination and Misidentification

Cell lines become contaminated when a foreign cell line or microorganism is introduced without the handler's knowledge. Although we do not wish to minimize the problem of microbial contamination, we will focus on cell line cross-contamination in this article. Cross-contamination may arise due to several causes, including poor technique (spread *via* aerosols or accidental contact), use of unplugged pipets, sharing media and reagents among cell lines and use of mitotically inactivated feeder layers or conditioned medium, which may carry contaminating cells if not properly eliminated, for example, by freeze-thaw and filtration.[11] In addition, a cell line can be replaced by another as a result of misidentification by confusing cultures during handling, mislabeling or poor freezer inventory control. Simple errors during labeling of culture flasks, truncation of the cell line name or typographic errors in a published manuscript, can result in significant confusion for years after the event when another researcher attempts to use the same cell line for ongoing experimental work.[12]

Cross-contamination may occur "early," in which case the original cell line has probably never existed independently, or "late," where the tested sample has been overgrown but other stocks of the original may still exist.[13] Unfortunately, cell lines generally become cross-contaminated early, while still within the originating laboratory.[14] This is not surprising: cultures can remain in crisis for a prolonged period of time before emergence of an immortalized population and this is a time when a single cell, if introduced from a separate cell line, would rapidly take over the culture.

There are now a number of studies pointing out the severity of this problem and the need to take urgent action to minimize cross-contamination and its consequences.[9,15–17] Ten years ago, the German Collection of Microorganisms and Cell Cultures (DSMZ) published data from its identification testing of cancer cell lines submitted by various laboratories for deposit at the cell bank.[14] They found that 18% of 252 submitted cell lines were cross-contaminated with more than half of cases arising within only 6 laboratories. Subsequent work by the DSMZ, extending the number of cell lines tested (Fig. 1), shows that of 598 leukemia–lymphoma cell lines (the group provided with the most complete genetic data), 187 (31%) were contaminated with Mycoplasma and/or a second cell line with 38 (6%) of cell lines contaminated with both. These data suggest that poor practice within some laboratories results in contamination of multiple cell lines with multiple contaminants, which can then be disseminated more widely if these cultures are used by others.

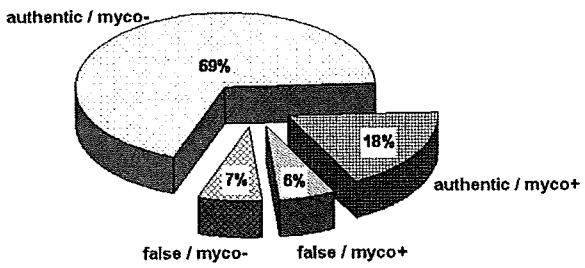

Figure 1. Rates of contamination for leukemia–lymphoma cell lines. Percentages of cross-contaminated and Mycoplasma-contaminated cell lines from a dataset of 598 leukemia and lymphoma cell lines analyzed by the German cell line bank DSMZ. "False/authentic" refers to the presence or absence of cross-contamination; "myco+/myco−" refers to the presence or absence of Mycoplasma contamination. Cell lines fall into the following categories: authentic/myco− (n = 411, 69%); authentic/myco+ (n = 108, 18%); false/myco− (n = 41, 7%) and false/myco+ (n = 38, 6%). (Courtesy of Hans Drexler, DSMZ.)

Other studies have pointed out that testing of cell lines is often infrequent, resulting in the failure to detect contaminated samples. John Ryan of Corning Life Sciences conducted surveys of seminar attendees in 1990, asking about Mycoplasma contamination; 50% were not currently performing testing and only 18% said they tested their cultures regularly. Almost 1 in 4 respondents (23%) had experienced Mycoplasma contamination, but with such a low level of testing, it is likely that the real figure was much higher.[18] Other data on cross-contamination were published in 2004 by researchers at the University of California, Berkeley, where Walter Nelson-Rees worked on this problem in the 1970s, focusing on the HeLa cell line.[19] Of 483 respondents to a questionnaire on cell line usage, 35% were using cell lines obtained from another laboratory rather than a cell line repository, but almost half of all respondents performed no testing for cross-contamination.[20]

A practical example of the consequences of cell line contamination can be found in a recent study published by Berglind *et al.*[21] The authors analyzed data within the UMD_p53 (2007) database, which includes information on the p53 status of 1,211 cell lines. Discrepancies were found in p53 status for 23% (88/384) of cell lines where data have been published by 2

independent laboratories. It is likely that many of these discrepancies arose due to work with cross-contaminated samples; the authors noted that many groups rely on previously published reports of a cell line's p53 status,[21] resulting in further confusion when interpreting results from these cell lines.

Cell banks have the expertise to detect such cross-contamination, and have been proactive in publishing reports of cross-contaminated cell lines,[22,23] in publishing test results online[24] and in developing new detection methods.[25–27] Unfortunately, however, cell banks have also reported reluctance from many researchers to deposit cell lines for distribution.[28] Such repositories specialize in the detection of cross-contamination and it is unlikely that most laboratories have comparable resources in this regard. In addition, many researchers obtain cell lines from one another, rather than approaching the originator or purchasing the cell line from a cell bank performing quality control testing. This may be faster or cheaper than obtaining cultures from a reputable source but the practice makes contamination more prevalent and harder to detect.

Practical Responses

Having defined the problems, it is time to focus on what can be done. Several cancer-related journals, including the International Journal of Cancer, have recently responded to these issues by changing their policies to require evidence of authentication with all submitted manuscripts using continuous cell lines.[29,30] Their response underscores the need for laboratories to come to grips with cell line cross-contamination and misidentification. Every researcher involved in cell culture will have cell lines currently in culture, stored in liquid nitrogen or may be commencing work on a new cell line. Put practically, how can you know if your cell lines are cross-contaminated?

There are 2 important answers to this question:

1. Check the literature, for example, by searching the PubMed database using the cell line name and "cross-contamination."
2. Check your cultured cells. Unless a cell line has come directly from a repository or other laboratory performing identification testing, it should be tested on arrival, and all cultures should be periodically tested while in use, before cryopreservation and when thawed from liquid nitrogen.[31] A variety of methods are available for authentication; for human cell lines, short tandem repeat (STR) profiling is the current international reference standard and is recommended as an easy and economical way to confirm cell line identity by comparison to donor tissue or to other samples of the cell line held by laboratories worldwide.[26]

Checking the Literature: A List of Cross-Contaminated Cell Lines

A 2004 survey of abstracts within the PubMed database would suggest that inappropriate usage of cross-contaminated cell lines is increasing,[20] despite many years of publication on this issue. It is possible that many researchers simply cannot find existing references to cross-contamination so, to make this already published work more accessible, we have surveyed the literature and other online resources for references to cell line contamination. The resulting list of cross-contaminated cell lines is included as Electronic Supporting Information.

To generate this list, the authors examined the PubMed database, references within other articles relating to this topic and the websites of 5 cell banks: the American Type Culture Collection (ATCC), DSMZ, European Collection of Cell Cultures (ECACC), Japanese Collection of Research Bioresources and the RIKEN Bioresource Center Cell Bank. A Wikipedia list of contaminated cell lines was also accessed (http://en.wikipedia.org/wiki/List_of_contaminated_cell_lines). Cross-contaminated cell lines are listed by name along with their species and cell type (both claimed and actual), the name of the contaminating cell line where identified, the reference in which this was reported and the PubMed ID number where available. Notes are also included for some cell lines. The list is made available in Excel spreadsheet or PDF format for easy accessibility.

The cell lines listed within this database are divided into 2 tables. Supporting Information Table 1 contains those cell lines where cross-contamination occurred as an early event, and thus where there is no original material remaining. Supporting Information Table 2 contains those cell lines where it is thought cross-contamination occurred as a late event and where original stocks may still exist. A full list of references is also given.

The current list of cross-contaminated cell lines (version 6.4) contains 360 cell lines, 346 in Supporting Information Table 1 and 14 in Supporting Information Table 2, drawn from 68 references. Cell lines affected are primarily human, although cultures from at least 8 other species are included, and come from a wide spectrum of tissue types. The cell or tumor type is given within the list where known; extensive work has been done by some cell banks and laboratories in this area to characterize the actual cell type or tumor type.[22,32] In some cases, this work has shown that a cell line carries the correct name but its cell or tumor type has been incorrectly identified, for example, the cell line RPMI-6666 was initially thought to have come from Hodgkin lymphoma but is now known to be an EBV-positive B-lymphoblastoid cell line.[22]

Common features for cross-contaminating cell lines within the current list are summarized in Table 1. It can be seen that most cross-contamination events have arisen from within the same species but a substantial minority (9%, 33/360) involved cross-contamination from a second species. For the intraspecies contaminants, all of those detected were human but it is likely that this relates to the difficulty of detecting intraspecies contaminants for nonhuman species. The commonest contaminant remains the HeLa cell line

Table 1. Cross-contaminating cell lines

Type of contaminant	Number of cell lines affected
Intraspecies	
Human	324
Nonhuman	0
Interspecies	33
Correct name—incorrect cell type (misidentified)[1]	3
Total	360
Contaminating cell line—12 most frequent	**Number of cell lines affected**
HeLa (human cervical adenocarcinoma)	106
T-24 (human bladder carcinoma)	18
HT-29 (human colon carcinoma)	12
CCRF-CEM (human acute lymphoblastic leukemia)	9
K-562 (human chronic myeloid leukemia)	9
U-937 (human lymphoma)	8
OCI/AML2 (human acute myeloid leukemia)	8
Hcu-10 (human esophageal carcinoma)[2]	7
M14 (human melanoma)	7
HL-60 (human acute myeloid leukemia)	6
PC3 (human prostate carcinoma)	6
SW-480, SW620 (human colon carcinoma)[3]	6

[1]For additional misidentified cell lines see Drexler *et al.*[22] [2]Hcu-10 carries the same genetic identity as Hcu-18, Hcu-22, Hcu-27, Hcu-33, Hcu-37 and Hcu-39; it is unclear which is the correct identity (see Electronic Supporting Information for reference). [3]SW480 and SW620 come from the same donor and therefore carry the same genetic identity (see Electronic Supporting Information for reference).

(29%, 106/360), followed by T-24 (5%, 18/360) and HT-29 (3%, 12/360).

It is important for such a list to be continually updated and feedback is welcome for this purpose. An earlier version of the database was released online by ECACC[31]; 6 cell banks have now agreed to make the database available online and to update this information where necessary. Current website addresses for access to the list of cross-contaminated cell lines are given in Table 2. In future, it is envisaged that the current list of misidentified cell lines will be included in a new initiative improving access to authentication data. The Standard Development Organization at the ATCC is in the process of producing an international standard for human cell line identification based on STR profiling (ATCC SDO Workgroup ASN-0002, manuscript submitted). Strict criteria for STR profiles derived from cancer cell lines are being developed. One consequence of this initiative is that funding is being sought for a quality controlled and curated cell line database with free access into which the database described here will be incorporated.

Table 2. Websites for ongoing access to the list of cross-contaminated cell lines

Cell bank	Website address
ATCC	http://www.atcc.org/
CellBank Australia	http://www.cellbankaustralia.com/
DSMZ	http://www.dsmz.de/
ECACC	http://www.hpacultures.org.uk/collections/ecacc.jsp
JCRB	http://cellbank.nibio.go.jp/
RIKEN Bioresource Center Cell Bank	http://www.brc.riken.go.jp/lab/cell/english/guide.shtml

Checking Your Cultures: Authentication of Cell Lines

Even if a search of the literature shows no indication that a cell line is contaminated, it is still essential to test the sample that you are working with. Authentication testing should be considered in a positive light, as an essential part of good cell culture practice[33] and as an assurance for researchers, funding bodies and journals that the cell line used is a valid experimental model.[17]

There are a number of methods for testing cell line identity. When the issue of cross-contamination was first identified, HeLa contaminants were detected through a combination of isoenzyme and chromosomal analysis.[19,34] Both techniques continue to be used but there are also many newer molecular approaches. Commonly used authentication methods are summarized in Table 3; what factors should be considered when choosing between these methods?

The expertise of the laboratory holding the cell line is an important factor. For example, laboratories with experience in cytogenetics would have the skills to identify species through karyotype analysis and cell lines through the presence or absence of appropriate markers.[35] Although this is an older approach, it still allows clear identification of cell lines, and many cell banks have published karyotypic information on their cell lines to allow comparison to well-characterized stocks. It should be noted that tumor-derived cell lines can be surprisingly difficult to harvest for cytogenetic analysis[35] and are typically heteroploid making interpretation difficult: the experience of the operator is important for success.

The species of cell lines held within the laboratory is also important. Although some authentication methods can be used on more than 1 species, molecular methods such as STR profiling are only successful for a single species; other species will simply fail to amplify.[26] This may not be an issue for laboratories working only with human samples but clearly is a significant factor for groups working with rodent cell lines. In this regard, multilocus DNA fingerprint analysis has a clear advantage, since probes are able to hybridize to a wide variety of species.[25] Unfortunately, although successful within a single laboratory, it can be challenging to compare DNA fingerprints across several experimental runs, and it is difficult to exchange data among laboratories or for cell

Table 3. Commonly used methods for authenticating cell lines

Name	Description	Purpose	References
Chromosomal analysis/karyotyping	Involves preparation of a metaphase spread with chromosome banding and painting to identify chromosome number and markers	Separates species, plus individual cell lines if detailed analysis performed	Ref. 35
Isoenzyme analysis	Biochemical method separating isoenzymes by electrophoresis; isoenzyme mobility may vary within or across species. Kits available include the Authentikit gel electrophoresis system	Separates species, sometimes individuals	Refs. 36,37
Multilocus DNA fingerprint analysis	Molecular method detecting variation in length within minisatellite DNA containing variable numbers of tandem repeat sequences. Analysis is by Southern blot hybridization using probes 33.6 and 33.15, M13 phage DNA, or oligonucleotide sequence	Separates individual cell lines across multiple species	Refs. 25,38
Short tandem repeat (STR) profiling	Molecular method detecting variation in length within microsatellite DNA containing variable numbers of short tandem repeat sequences. Analysis is by PCR with comparison to set size standards; usually available in a kit format allowing amplification of up to 16 loci	Separates individual cell lines within a single species	Refs. 26,39
Polymerase chain reaction (PCR) fragment analysis	Molecular method involving amplification of specific genes or gene families, aiming to detect variations in exon/intron sequence, transcript splicing, or the presence of pseudogenes. Genes examined include the aldolase gene family and the beta-globin gene	Separates species only	Refs. 40,41
Sequencing of "DNA barcode" regions	Involves sequencing of a DNA fragment from the mitochondrial gene cytochrome *c* oxidase subunit I, with comparison to sequence obtained from online databases. This "DNA barcode" has been shown in practice to distinguish a broad range of animal species	Separates species only	Refs. 27,42

banks to publish such fingerprints online. It is advisable to always compare the test sample to a known sample within the same experiment, ideally using DNA from the blood or tissue of the original donor.

The obvious advantage of STR profiling lies in the use of control samples to generate a numerical code for each sample, which precisely identifies that cell line and which can be readily shared and published online. It is primarily for this reason that STR profiling is recommended as an international reference standard for human cell lines[26] and accepted within the legal system for human identity testing.[39] STR profiling is based on the presence of STRs within the human genome that exist at variable lengths throughout the population. Each of the repeat regions to be analyzed (usually tetra or pentanucleotide repeats in noncoding sequence) is amplified by PCR using primers carrying fluorescent tags and electrophoresed in a sequencing gel; the precise length of each allele is determined and compared with size standards and controls. This allows identification software to assign a number to each allele at that locus (see, *e.g.*, Fig. 2). The combination of multiple loci—classically 13, as used in the FBI Laboratory's Combined DNA Index System (CODIS)—gives sufficient data to uniquely identify that individual.

STR profiles for individual cell lines and panels have now been reported by many laboratories (*e.g.*, Ref. 44) and are published online by several cell banks. However, there are some cautions to be aware of when using this approach. It is accepted within the forensic field that tumor samples are not as genetically stable as other tissue sources for STR profiling, because of loss of heterozygosity and microsatellite instability.[45,46] This is even more evident in tumor-derived cell lines, where evolution or genetic drift continues to occur with passage.[47] When searching an online database of STR profiles from cell lines, the user needs to look for close matches and not just identical matches; most studies would agree that 80% similarity is an appropriate threshold for declaring a match when comparing cell line profiles.[26,44] There may also be a significant start-up cost if testing in-house; in addition to an STR kit, access to methods for DNA extraction, precise quantitation, fragment analysis and software for STR profile identification is required.

The fact that STR profiling is only suitable for distinguishing cell lines of a single species has led to the need to re-examine authentication of nonhuman cell lines. Laboratory rodent samples will always be difficult to identify precisely due to inbreeding; laboratories working with rat or mouse cultures may wish to examine strain identity rather than authentication of individual cell lines, particularly if they have expertise in single nucleotide polymorphism (SNP) or single sequence length polymorphism (SSLP) analysis,

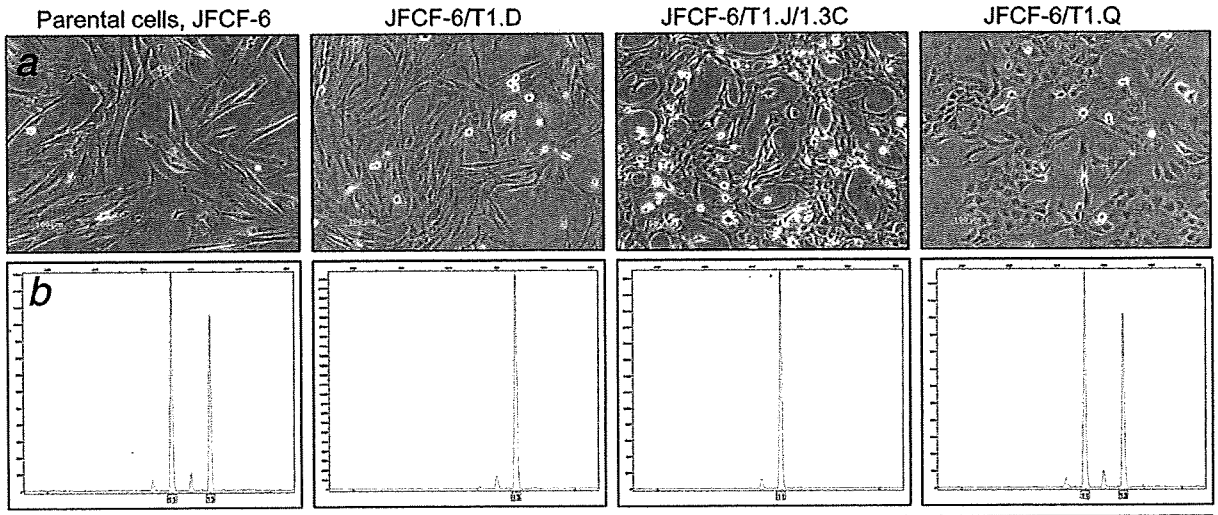

c

Cell Line	D8S1179	D21S11	D7S820	CSF1PO	D3S1358	TH01	D13S317	D16S539	D2S1338	D19S433	vWA	TPOX	D18S51	Amel	D5S818	FGA
Parental	10,13	29,31	11	10,13	14,16	9.3	8,12	11,13	17,20	14,15	16,17	11	12,19	X,Y	9,11	21
JFCF-6/ T1.D	13	29,31	11	10,13	14	9.3	8	13	17,20	14,15	16,17	11	12,19	X,Y	9,11	21
JFCF-6/ T1.J/1.3C	10,13	29,31	11	10,13	14,16	9.3	8,12	11	17,20	14,15	16,17	11	12,19	X,Y	9,11	21
JFCF-6/ T1.Q	10,13	29,31	11	10,13	14,16	9.3	8,12	11,13	17,20	14,15	16,17	11	19	X,Y	9,11	21

Figure 2. Example of STR profile generation and interpretation. An example of STR profiling is given for the JFCF-6 cell fibroblast strain and 3 of its immortalized derivatives, JFCF-6/T1.D, JFCF-6/T1.J/1.3C and JFCF-6/T1.Q.[43] Derivatives were established after transfection with SV40 early region DNA and were handled by CellBank Australia through its Culture and Return service. DNA from each culture was amplified using the AmpFlSTR Identifiler PCR Amplification Kit (Applied Biosystems, Mulgrave, Australia), which includes primers for 16 STR loci. Amplified sequence was analyzed using an ABI PRISM 3100 Genetic Analyzer and data files were assessed using GeneMapper ID software (Applied Biosystems). (*a*) Photographs taken of each culture, comparing parental cells to the morphology of each derived cell line (scale bar = 100 μm). Each derivative has a markedly different morphology, showing the need for authentication testing to confirm that derivatives correspond to the parental strain. (*b*) Examples of STR peak amplification for the D16S539 locus of each culture. Amplification varies at this locus due to genetic drift during establishment of the 3 JFCF-6–derived cell lines. The peaks shown correspond to specific allele sizes known to exist at this locus and confirmed using size standards and controls supplied with the kit (data not shown). (*c*). STR profiles for JFCF-6 and derived cell lines; the locus shown in B, D16S539, is highlighted in grey. Despite the differences seen due to genetic drift, the profiles for derived lines closely match the parental cell strain and all of these cultures are correctly identified.

which can be used for strain identification.[48,49] SNP analysis can also be used to identify individual samples[50] and has been used for cell line authentication,[51] making it a method of great promise for application to human and nonhuman samples alike. Laboratories working on specific cell types may be able to use expressed markers for identification, as 1 laboratory has done recently, publishing a technique for identification of hybridomas based on sequencing of light-chain variable regions.[52]

A simple method has recently emerged to help detect interspecies contamination. The term DNA barcoding here refers to amplifying a specific 648 bp fragment of the mitochondrial gene, cytochrome *C* oxidase subunit I (COI), using primers developed by Folmer *et al.*[53] Sequence divergences within this fragment allow species discrimination across almost all animal phyla.[42] Although debate is ongoing as to whether DNA barcoding is sufficient for assignment of species in taxonomic terms,[54] it is clear that the technique can readily identify the species of an unknown specimen if compared with previously sequenced reference material in online databases.[55] DNA barcoding has been tested for species identification of cell lines[27] and its use would reduce the incidence of interspecies cell line

contamination, found here to cause almost 1 in 10 of all published cross-contamination events.

Whatever the authentication method used, it should be clearly recorded within the researcher's experimental notes, and the result should be linked if possible to the laboratory's liquid nitrogen records, so that quality control for frozen vials is clearly evident. When publishing experimental work, the Material and Methods section should include the correct and full name of the cell line used, its origin (with appropriate references), the source of the cultures used and details of authentication testing.

Conclusions

Cell line contamination is a serious issue that detracts from the use of cell lines as model systems to help us understand a broad range of diseases, including cancer. Responding practically by checking each cell line before it is used, searching for previous references and authenticating the sample itself is worthwhile and will reduce the risk and subsequent consequences of contamination long-term.

Acknowledgements

The authors gratefully acknowledge the work of many cell banks and laboratories working in this area, and those responsible for compiling the list in Wikipedia, and regret that there is insufficient space to include all references here. A complete list of publications on cross-contamination can be found in the Electronic Supporting Information. Elsa Moy is thanked for her work in handling the cell lines shown in Figure 2. CellBank Australia was established by a joint venture of the Children's Medical Research Institute, Cure Cancer Australia Foundation and National Breast Cancer Foundation, and by an Enabling Grant of the National Health and Medical Research Council of Australia.

References

1. Hanahan D, Weinberg RA. The hallmarks of cancer. *Cell* 2000;100:57–70.
2. Wistuba II, Behrens C, Milchgrub S, Syed S, Ahmadian M, Virmani AK, Kurvari V, Cunningham TH, Ashfaq R, Minna JD, Gazdar AF. Comparison of features of human breast cancer cell lines and their corresponding tumors. *Clin Cancer Res* 1998;4:2931–8.
3. Ross DT, Scherf U, Eisen MB, Perou CM, Rees C, Spellman P, Iyer V, Jeffrey SS, Van de RM, Waltham M, Pergamenschikov A, Lee JC, et al. Systematic variation in gene expression patterns in human cancer cell lines. *Nat Genet* 2000;24: 227–35.
4. Jones S, Chen WD, Parmigiani G, Diehl F, Beerenwinkel N, Antal T, Traulsen A, Nowak MA, Siegel C, Velculescu VE, Kinzler KW, Vogelstein B, et al. Comparative lesion sequencing provides insights into tumor evolution. *Proc Natl Acad Sci USA* 2008;105:4283–8.
5. Reddel RR. The role of senescence and immortalization in carcinogenesis. *Carcinogenesis* 2000;21:477–84.
6. Boehm JS, Hahn WC. Immortalized cells as experimental models to study cancer. *Cytotechnology* 2004;45:47–59.
7. Masters JR. Human cancer cell lines: fact and fantasy. *Nat Rev Mol Cell Biol* 2000;1: 233–6.
8. MacLeod RA, Nagel S, Scherr M, Schneider B, Dirks WG, Uphoff CC, Quentmeier H, Drexler HG. Human leukemia and lymphoma cell lines as models and resources. *Curr Med Chem* 2008;15:339–59.
9. Hughes P, Marshall D, Reid Y, Parkes H, Gelber C. The costs of using unauthenticated, over-passaged cell lines: how much more data do we need? *Biotechniques* 2007;43:575, 577–2.
10. van Staveren WC, Solis DY, Hebrant A, Detours V, Dumont JE, Maenhaut C. Human cancer cell lines: experimental models for cancer cells in situ? For cancer stem cells? *Biochim Biophys Acta* 2009; 1795:92–103.
11. van Pelt JF, Decorte R, Yap PS, Fevery J. Identification of HepG2 variant cell lines by short tandem repeat (STR) analysis. *Mol Cell Biochem* 2003;243:49–54.
12. Shimada Y. Researchers should have respect for the originator of the cell lines. *Clin Cancer Res* 2005;11:4634.
13. Drexler HG, Uphoff CC, Dirks WG, MacLeod RA. Mix-ups and mycoplasma: the enemies within. *Leuk Res* 2002;26: 329–33.
14. MacLeod RA, Dirks WG, Matsuo Y, Kaufmann M, Milch H, Drexler HG. Widespread intraspecies cross-contamination of human tumor cell lines arising at source. *Int J Cancer* 1999;83: 555–63.
15. Stacey GN. Cell contamination leads to inaccurate data: we must take action now. *Nature* 2000;403:356.
16. Masters JR. False cell lines: the problem and a solution. *Cytotechnology* 2002;39:69–74.
17. Nardone RM. Eradication of cross-contaminated cell lines: a call for action. *Cell Biol Toxicol* 2007;23:367–72.
18. Ryan JA. Understanding and managing cell culture contamination. Corning Technical Bulletin 1994. Available at: http://catalog2.corning.com/Lifesciences/media/pdf/cccontamination.pdf accessed on 18 August 2009.
19. Nelson-Rees WA, Flandermeyer RR. HeLa cultures defined. *Science* 1976;191: 96–8.
20. Buehring GC, Eby EA, Eby MJ. Cell line cross-contamination: how aware are mammalian cell culturists of the problem and how to monitor it? *In Vitro Cell Dev Biol Anim* 2004;40:211–5.
21. Berglind H, Pawitan Y, Kato S, Ishioka C, Soussi T. Analysis of p53 mutation status in human cancer cell lines: a paradigm for cell line cross-contamination. *Cancer Biol Ther* 2008;7:699–708.
22. Drexler HG, Dirks WG, Matsuo Y, MacLeod RA. False leukemia-lymphoma cell lines: an update on over 500 cell lines. *Leukemia* 2003;17:416–26.
23. Yoshino K, Iimura E, Saijo K, Iwase S, Fukami K, Ohno T, Obata Y, Nakamura Y. Essential role for gene profiling analysis in the authentication of human cell lines. *Hum Cell* 2006;19:43–8.
24. Dirks WG, MacLeod RA, Nakamura Y, Kohara A, Reid Y, Milch H, Drexler HG, Mizusawa H. Cell line cross-contamination initiative: an interactive reference database of STR profiles covering common cancer cell lines. *Int J Cancer* 2010;126:303–4.
25. Stacey GN, Bolton BJ, Morgan D, Clark SA, Doyle A. Multilocus DNA fingerprint analysis of cell banks: stability studies and culture identification in human B-lymphoblastoid and mammalian cell lines. *Cytotechnology* 1992;8:13–20.
26. Masters JR, Thomson JA, ly-Burns B, Reid YA, Dirks WG, Packer P, Toji LH, Ohno T, Tanabe H, Arlett CF, Kelland LR, Harrison M, et al. Short tandem repeat profiling provides an international reference standard for human cell lines. *Proc Natl Acad Sci USA* 2001;98: 8012–17.
27. Cooper JK, Sykes G, King S, Cottrill K, Ivanova NV, Hanner R, Ikonomi P. Species identification in cell culture: a two-pronged molecular approach. *In Vitro Cell Dev Biol Anim* 2007;43:344–51.
28. MacLeod RA, Drexler HG. Public repositories: users reluctant to give materials. *Nature* 2006;439:912.

29. Potash J, Anderson KC. What's your line? *Clin Cancer Res* 2009;15:4251.
30. Lichter P, Allgayer H, Bartsch H, Fusenig N, Hemminki K, von Knebel DM, Kyewski B, Miller AB, zur HH. Obligation for cell line authentication: appeal for concerted action. *Int J Cancer* 2010;126:1.
31. Freshney RI. Database of misidentified cell lines. *Int J Cancer* 2010;126:302.
32. Schweppe RE, Klopper JP, Korch C, Pugazhenthi U, Benezra M, Knauf JA, Fagin JA, Marlow LA, Copland JA, Smallridge RC, Haugen BR. Deoxyribonucleic acid profiling analysis of 40 human thyroid cancer cell lines reveals cross-contamination resulting in cell line redundancy and misidentification. *J Clin Endocrinol Metab* 2008;93:4331–41.
33. Balls M, Coecke S, Bowe G, Davis J, Gstraunthaler G, Hartung T, Hay R, Merten OW, Price A, Schechtman LM, Stacey G, Stokes W. The importance of Good Cell Culture Practice (GCCP). *ALTEX* 2006;23 Suppl.:270–3.
34. Gartler SM. Genetic markers as tracers in cell culture. *Natl Cancer Inst Monogr* 1967; 26:167–95.
35. MacLeod RA, Kaufmann M, Drexler HG. Cytogenetic harvesting of commonly used tumor cell lines. *Nat Protoc* 2007;2: 372–82.
36. O'Brien SJ, Shannon JE, Gail MH. A molecular approach to the identification and individualization of human and animal cells in culture: isozyme and allozyme genetic signatures. *In Vitro* 1980;16: 119–35.
37. Stacey GN, Hoelzl H, Stephenson JR, Doyle A. Authentication of animal cell cultures by direct visualization of repetitive DNA, aldolase gene PCR and isoenzyme analysis. *Biologicals* 1997;25:75–85.
38. Jeffreys AJ, Wilson V, Thein SL. Hypervariable "minisatellite" regions in human DNA. *Nature* 1985;314:67–73.
39. Butler JM. Genetics and genomics of core short tandem repeat loci used in human identity testing. *J Forensic Sci* 2006;51:253–65.
40. Liu M, Liu H, Tang X, Vafai A. Rapid identification and authentication of closely related animal cell culture by polymerase chain reaction. *In Vitro Cell Dev Biol Anim* 2008;44:224–7.
41. Steube KG, Koelz AL, Drexler HG. Identification and verification of rodent cell lines by polymerase chain reaction. *Cytotechnology* 2008;56:49–56.
42. Hebert PD, Cywinska A, Ball SL, deWaard JR. Biological identifications through DNA barcodes. *Proc Biol Sci* 2003;270:313–21.
43. Jiang WQ, Zhong ZH, Nguyen A, Henson JD, Toouli CD, Braithwaite AW, Reddel RR. Induction of alternative lengthening of telomeres-associated PML bodies by p53/ p21 requires HP1 proteins. *J Cell Biol* 2009;185:797–810.
44. Lorenzi PL, Reinhold WC, Varma S, Hutchinson AA, Pommier Y, Chanock SJ, Weinstein JN. DNA fingerprinting of the NCI-60 cell line panel. *Mol Cancer Ther* 2009;8:713–24.
45. Poetsch M, Petersmann A, Woenckhaus C, Protzel C, Dittberner T, Lignitz E, Kleist B. Evaluation of allelic alterations in short tandem repeats in different kinds of solid tumors–possible pitfalls in forensic casework. *Forensic Sci Int* 2004;145:1–6.
46. Vauhkonen H, Hedman M, Vauhkonen M, Kataja M, Sipponen P, Sajantila A. Evaluation of gastrointestinal cancer tissues as a source of genetic information for forensic investigations by using STRs. *Forensic Sci Int* 2004;139:159–67.
47. Parson W, Kirchebner R, Muhlmann R, Renner K, Kofler A, Schmidt S, Kofler R. Cancer cell line identification by short tandem repeat profiling: power and limitations. *FASEB J* 2005;19:434–6.
48. Witmer PD, Doheny KF, Adams MK, Boehm CD, Dizon JS, Goldstein JL, Templeton TM, Wheaton AM, Dong PN, Pugh EW, Nussbaum RL, Hunter K, et al. The development of a highly informative mouse Simple Sequence Length Polymorphism (SSLP) marker set and construction of a mouse family tree using parsimony analysis. *Genome Res* 2003;13: 485–91.
49. Petkov PM, Cassell MA, Sargent EE, Donnelly CJ, Robinson P, Crew V, Asquith S, Haar RV, Wiles MV. Development of a SNP genotyping panel for genetic monitoring of the laboratory mouse. *Genomics* 2004;83: 902–11.
50. Pakstis AJ, Speed WC, Fang R, Hyland FC, Furtado MR, Kidd JR, Kidd KK. SNPs for a universal individual identification panel. *Hum Genet* 2010;127:315–24.
51. Demichelis F, Greulich H, Macoska JA, Beroukhim R, Sellers WR, Garraway L, Rubin MA. SNP panel identification assay (SPIA): a genetic-based assay for the identification of cell lines. *Nucleic Acids Res* 2008;36:2446–56.
52. Koren S, Kosmac M, Colja VA, Montanic S, Curin SV. Antibody variable-region sequencing as a method for hybridoma cell-line authentication. *Appl Microbiol Biotechnol* 2008;78:1071–8.
53. Folmer O, Black M, Hoeh W, Lutz R, Vrijenhoek R. DNA primers for amplification of mitochondrial cytochrome c oxidase subunit I from diverse metazoan invertebrates. *Mol Mar Biol Biotechnol* 1994;3:294–9.
54. Linares MC, Soto-Calderon ID, Lees DC, Anthony NM. High mitochondrial diversity in geographically widespread butterflies of Madagascar: a test of the DNA barcoding approach. *Mol Phylogenet Evol* 2009;50:485–95.
55. Dawnay N, Ogden R, McEwing R, Carvalho GR, Thorpe RS. Validation of the barcoding gene COI for use in forensic genetic species identification. *Forensic Sci Int* 2007;173:1–6.

THE JOURNAL OF BIOLOGICAL CHEMISTRY VOL. 283, NO. 38, pp. 26089–26097, September 19, 2008

Double Deficiency of Tetraspanins CD9 and CD81 Alters Cell Motility and Protease Production of Macrophages and Causes Chronic Obstructive Pulmonary Disease-like Phenotype in Mice*[S]

Received for publication, March 10, 2008, and in revised form, July 7, 2008 Published, JBC Papers in Press, July 28, 2008, DOI 10.1074/jbc.M801902200

Yoshito Takeda[‡1], Ping He[‡§1], Isao Tachibana[‡2], Bo Zhou[‡], Kenji Miyado[¶3], Hideshi Kaneko[‖], Mayumi Suzuki[‡], Seigo Minami[‡], Takeo Iwasaki[‡], Sho Goya[‡], Takashi Kijima[‡], Toru Kumagai[‡], Mitsuhiro Yoshida[‡], Tadashi Osaki[‡], Toshihisa Komori[‡4], Eisuke Mekada[¶], and Ichiro Kawase[‡]

From the [‡]Department of Respiratory Medicine, Allergy and Rheumatic Diseases, Osaka University Graduate School of Medicine, Osaka 565-0871, Japan, the [§]Department of Respiratory Medicine, the Second Affiliated Hospital, School of Medicine, Xi'an Jiaotong University, Xi'an, 71004 China, [¶]Research Institute for Microbial Diseases, Osaka University, Osaka 565-0871, Japan, and [‖]Pharmacological and Safety Research Department, Pharmaceutical Development Research Laboratories, Teijin Pharma Limited, Tokyo 191-8512, Japan

CD9 and CD81 are closely related tetraspanins that regulate cell motility and signaling by facilitating the organization of multimolecular membrane complexes, including integrins. We show that CD9 and CD81 are down-regulated in smoking-related inflammatory response of a macrophage line, RAW264.7. When functions of CD9 and CD81 were ablated with monoclonal antibody treatment, small interfering RNA transfection, or gene knock-out, macrophages were less motile and produced larger amounts of matrix metalloproteinase (MMP)-2 and MMP-9 than control cells *in vitro*. In line with this, CD9/CD81 double-knock-out mice spontaneously developed pulmonary emphysema, a major pathological component of chronic obstructive pulmonary disease (COPD). The mutant lung contained an increased number of alveolar macrophages with elevated activities of MMP-2 and MMP-9 and progressively displayed enlarged airspace and disruption of elastic fibers in the alveoli. Secretory cell metaplasia, a finding similar to goblet cell metaplasia in cigarette smokers, was also observed in the epithelium of terminal bronchioles. With aging, the double-knock-out mice showed extrapulmonary phenotypes, including weight loss, kyphosis, and osteopenia. These results suggest that the tetraspanins CD9 and CD81 regulate cell motility and protease production of macrophages and that their dysfunction may underlie the progression of COPD.

Chronic obstructive pulmonary disease (COPD),[5] a disease defined by incompletely reversible airflow limitation, results from abnormal inflammatory response to chronic cigarette smoking. Pulmonary emphysema is a major component of COPD, and a dominant hypothesis in its pathophysiology is that persistent infiltration of inflammatory cells and production of proteases, including matrix metalloproteinases (MMPs) in the lung, lead to tissue destruction and airspace enlargement (1, 2). In patients with emphysema, there was an increase in bronchoalveolar lavage fluid (BALF) concentrations and macrophage expression of MMP-9 (3). Studies of human samples have shown increases of MMP-2 and MMP-9 in smoking-related emphysema (4). Alveolar macrophages secrete elastolytic enzymes, including MMP-2, MMP-9, and MMP-12, and play a pivotal role in the pathophysiology of COPD. There was a marked increase in the numbers of macrophages in airways, lung parenchyma, BALF, and sputum in patients with emphysema (2). Macrophages are activated by cigarette smoke to release inflammatory mediators such as TNF-α, chemokines, and reactive oxygen species as well as MMPs, providing a cellular mechanism that links smoking with inflammation in COPD (2). It was recently proposed that lowered activity of histone deacetylases (HDACs), which are suppressors of inflammatory genes, accounts for the persistent activation of macrophages in COPD patients (5).

The tetraspanin proteins include at least 33 members, including CD9, CD63, CD81, CD82, and CD151 in mammals. They are characterized by the structure that spans the plasma membrane four times and have a propensity to form complexes with each other and with other functional molecules, including

* This work was supported by a grant from Takeda Science Foundation, Osaka, Japan (to I. T.), and a grant from "Kansai Biomedical Cluster" Project in Saito, Japan, which is promoted by the Knowledge Cluster Initiative of the Ministry of Education, Culture, Sports, Science and Technology, Japan (to I. T.). The costs of publication of this article were defrayed in part by the payment of page charges. This article must therefore be hereby marked "*advertisement*" in accordance with 18 U.S.C. Section 1734 solely to indicate this fact.

[S] The on-line version of this article (available at http://www.jbc.org) contains supplemental Experimental Procedures, Figs. 1–4, Tables 1 and 2, and Video 1.

[1] Both authors contributed equally to this work.

[2] To whom correspondence should be addressed: Dept. of Respiratory Medicine, Allergy and Rheumatic Diseases, Osaka University Graduate School of Medicine, Osaka 565-0871, Japan. Tel.: 81-6-6879-3833; Fax: 81-6-6879-3839; E-mail: itachi02@imed3.med.osaka-u.ac.jp.

[3] Present address: Dept. of Reproductive Biology and Pathology, National Center for Child Health and Development, Tokyo 157-8535, Japan.

[4] Present address: Division of Cell Biology, Dept. of Basic Medical Sciences, Nagasaki University Graduate School of Biomedical Sciences, Nagasaki 852-8588, Japan.

[5] The abbreviations used are: COPD, chronic obstructive pulmonary disease; MMP, matrix metalloproteinase; BALF, bronchoalveolar lavage fluid; HDAC, histone deacetylase; KO, knock-out; DKO, double-knock-out; TSA, trichostatin A; CSE, cigarette smoke extract; TIMP, tissue inhibitor of metalloproteinase; FN, fibronectin; BMDM, bone marrow-derived macrophage; pQCT, peripheral quantitative computed tomography; IFN, interferon; mAb, monoclonal antibody; siRNA, small interfering RNA; DMEM, Dulbecco's modified Eagle's medium; FBS, fetal bovine serum; WT, wild type; RT, reverse transcription; TNF-α, tumor necrosis factor-α; PAS, periodic acid-Schiff.

integrins, signaling proteins, and membrane-anchored growth factors at specialized membrane microdomains. As organizer of these multimeric complexes, tetraspanins regulate cell morphology, motility, invasion, fusion, and signaling (6). It has been increasingly recognized that tetraspanin-integrin complexes also regulate the production of MMPs, particularly in tumor cells. Treatment of a breast cancer cell line with anti-tetraspanin monoclonal antibodies (mAbs) stimulated production of MMP-2 and formation of invasive protrusions (7). CD9 expression inhibited integrin-dependent morphologic differentiation and MMP-2 production of small cell lung cancer cells via the phosphatidylinositol 3-kinase/Akt pathway (8). Overexpression of CD81 or CD82 reduced cell motility and MMP-9 activity in multiple myeloma cell lines (9). However, their role in motility and MMP production of macrophage has yet to be studied.

In this study, our *in vitro* experiments show that CD9 and CD81, the two widely distributed and closely correlated tetraspanins, are down-regulated in smoking-related inflammatory response of macrophages and that ablation of their function suppresses cell motility and increases the production of MMPs. Moreover, *in vivo* experiments using CD9/CD81 double-knock-out (DKO) mice displayed accumulation of macrophages and increased activities of MMPs in the mutant lung. The DKO mice progressively developed pulmonary emphysema, weight loss, and osteopenia, a phenotype akin to human COPD.

EXPERIMENTAL PROCEDURES

Immunoblotting—A mouse macrophage line, RAW264.7, and a human alveolar epithelial cell line, A549, were serum-starved for 24 h and treated with 10 ng/ml trichostatin A (TSA; Wako Pure Chemical Industries, Osaka, Japan) or 0.1% cigarette smoke extract (CSE) as described previously (10) for 48 h. In some experiments, 10 μM theophylline (Wako Pure Chemical Industries) or 1 μM dexamethasone (Sigma) were co-added with TSA into the culture. Cells were lysed in lysis buffer containing 1% Brij99, 25 mM HEPES (pH 7.5), 150 mM NaCl, 5 mM $MgCl_2$, 2 mM phenylmethylsulfonyl fluoride, 10 μg/ml aprotinin, and 10 μg/ml leupeptin. Cell lysates were separated by SDS-PAGE, transferred to polyvinylidene difluoride membranes, and probed with rat anti-mouse CD9 (KMC8) and integrin β1 (KMI6) mAbs (BD Biosciences) and hamster anti-mouse CD81 mAb (Eat2; AbD Serotec, Oxford, UK). For A549 lysates, mouse anti-human CD9 (MM2/57; BIOSOURCE) and CD81 (JS64; Immunotech, Marseille, France) mAbs were used.

Treatment of RAW264.7 Cells with mAbs or Small Interfering RNA (siRNA) Transfection against CD9 and CD81—To test the effects of function-inhibitory mAbs to CD9 (KMC8) and CD81 (2F7; Southern Biotechnology, Birmingham, AL), RAW264.7 cells were cultured in DMEM containing 0.1% FBS for 24 h in the absence or presence of 20 μg/ml of IgG (isotype matched with KMC8), KMC8, 2F7, and KMC8 plus 2F7. mRNA was extracted, and expressions of MMP-2, MMP-9, MMP-12, tissue inhibitor of metalloproteinase (TIMP)-1, and TIMP-2 were evaluated by reverse transcription (RT)-PCR as described previously (11, 12). Culture supernatants were studied for MMP-9 activity in gelatin zymography. The activities were quantified on a FluorChem using software AlphaEase (Alpha Innotech, San Leandro, CA). In a cell migration assay, RAW264.7 cells (5×10^4) suspended in serum-free DMEM and preincubated with the mAbs were applied to the upper chamber of fibronectin (FN)-precoated Transwells. DMEM containing 10% FBS was added to the lower chamber. After 4 h, cells migrating to the lower surface were counted with Diff-Quick stain (International Reagents, Hyogo, Japan). For siRNA transfection, RAW264.7 cells were transfected with mixture siRNAs against mouse CD9 or CD81 (B-Bridge International, Sunnyvale, CA) or control mixture RNAs (B-Bridge International) using Lipofectamine 2000 (Invitrogen). Gene silencing effects were confirmed by immunoblotting. The cells were cultured for 24 h in serum-free DMEM, and the culture supernatants were studied for MMP-9 activity by gelatin zymography.

Mice—The generation of CD9/CD81 DKO mice was described previously (13). These mice were backcrossed into the C57BL/6J background. The genotyping of littermates was achieved by PCR analysis. All animal experiments were performed with age- and sex-matched littermate controls using at least three animals at each time point. The mice were maintained in a specific pathogen-free facility, and all animal procedures were performed in accordance with the Osaka University guidelines on Animal Care.

Histology and Histomorphometric Analysis of the Lung—Lungs were inflated to 25 cm of water pressure with 10% buffered neutral formalin via an intratracheal cannula and embedded in paraffin. Parasagittal 5-μm-thick sections were stained with hematoxylin and eosin. Elastica-van Gieson stain for elastin, Masson's trichrome stain for collagen, and Alcian blue/periodic acid-Schiff (PAS) stain for mucus-secreting cells were also performed. Airspace size was quantified by calculating the mean chord length using the NIH Image software (14). Briefly, a minimum of 10 fields from each mouse lung was randomly acquired and visualized using the program Scion Image (Scion, Frederick, MD). The images were subject to sequential logical image match and operations with a horizontal and vertical grid. At least 200 measurements per field were made, and the length of the lines overlying airspace was averaged as the mean chord length.

Bronchoalveolar Lavage and Gelatin Zymography—Lungs of anesthetized mice were subjected to lavage with 3 volumes of 1 ml of phosphate-buffered saline containing 0.1% bovine serum albumin. Collected cells in the BALF were centrifuged onto Cytospin slides and visualized by Diff-Quick stain. Total cell counts and their subsets were determined using a hemocytometer. The supernatants of BALF were concentrated 10-fold using Centricon 10 filtration units (Millipore, Bedford, MA). Samples containing an equal amount of protein were electrophoresed in 10% zymogram gelatin gels (NOVEX, Carlsbad, CA). Gels were washed twice in 2.5% Triton X-100, incubated for 24 h with 40 mM Tris/HCl (pH 7.5), 10 mM $CaCl_2$, and 1 μM $ZnCl_2$, and stained with Coomassie Blue. Gelatinolytic activities were quantified on a FluorChem using software AlphaEase. The identical gels were treated in the presence of 0.01 M EDTA in parallel, and metal dependence, which is characteristic of MMPs, was confirmed by disappearance of lytic bands.

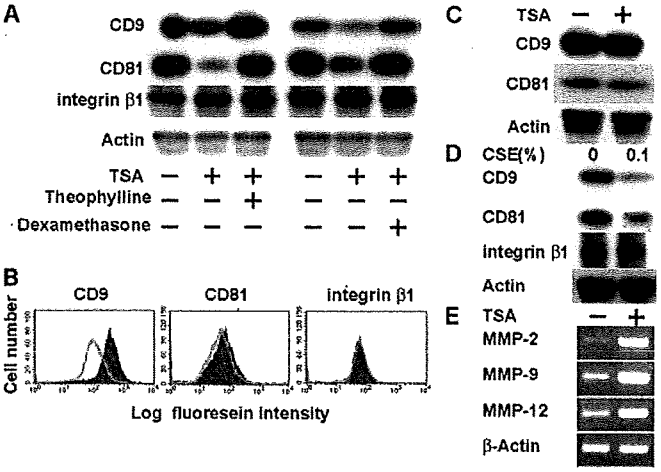

FIGURE 1. **TSA or CSE down-regulates CD9 and CD81 while up-regulating MMPs in RAW264.7 macrophages.** *A*, RAW264.7 cells were cultured in the absence or presence of TSA, theophylline, and dexamethasone for 48 h. Expressions of CD9, CD81, and integrin β1 were examined by immunoblotting using whole cell lysates. Anti-actin blots confirm equal amounts of protein loaded in each lane. *B*, RAW264.7 was cultured in the absence (*filled histograms*) or presence (*open histograms*) of TSA. Surface expressions of CD9, CD81, and integrin β1 were analyzed by flow cytometry. *C*, A549 alveolar epithelial cells were cultured in the absence or presence of TSA. CD9 and CD81 were immunoblotted. *D*, RAW264.7 was cultured in the absence or presence of 0.1% CSE for 48 h. CD9, CD81, and integrin β1 were immunoblotted. *E*, RAW264.7 was cultured in the absence or presence of TSA. Expressions of MMP-2, MMP-9, and MMP-12 were analyzed by RT-PCR. β-Actin amplification was internal control.

Peripheral Quantitative Computed Tomography (pQCT) Analysis—Femurs were fixed with 10% buffered formalin and measured using an XCT Research SA (Stratec Medizintechnik, Pforzheim, Germany) as described previously (15). The contour of the total bone was determined automatically with the pQCT software algorithm. The cortical and trabecular parameters were obtained at the diaphysis and 2 mm from distal epiphysis, respectively. The total mineral content and strength strain index were determined as described previously (16).

RESULTS

CD9 and CD81 Are Down-regulated by Smoking-related Inflammatory Stimuli in RAW264.7 Macrophages—Cigarette smoke reduces the expression and activity of HDACs in macrophages of COPD patients, resulting in amplification of pro-inflammatory gene transcription (5). To examine the effect of lowered HDAC activities on CD9 and CD81 expression, RAW264.7 macrophages were cultured in the presence of a HDAC inhibitor, TSA. As shown in Fig. 1*A*, treatment of RAW264.7 with TSA induced a decrease in protein levels of CD9 and CD81. The effects were reversed by the addition of a low concentration of HDAC activators, theophylline and dexamethasone (17), suggesting that their down-regulation was specific to HDAC inactivation and not because of nonspecific cytotoxicity of 10 ng/ml TSA. As a control, we tested the expression of integrin β1 but found no change in the presence of these agents (Fig. 1*A*). Consistent with the immunoblotting data, flow cytometry showed that TSA decreases surface expressions of CD9 and, to a lesser extent, CD81 while not affecting integrin β1 (Fig. 1*B*). The inhibitory effect of TSA was not observed in an alveolar epithelial cell line, A549 (Fig. 1*C*). We also examined the effect of IFN-γ and TNF-α, which are pro-inflammatory cytokines elevated in smoke-induced inflammation (18), on RAW264.7. As shown in supplemental Fig. 1, although TNF-α had no effect, IFN-γ dose-dependently suppressed the expressions of CD9 and CD81. Finally, we directly treated RAW264.7 cells with CSE (10) and observed that 0.1% CSE similarly reduced CD9 and CD81 but not integrin β1 in immunoblotting (Fig. 1*D*) and flow cytometry (data not shown). These results suggest that cigarette smoke may induce macrophages to down-regulate CD9 and CD81 expression in a cell-autonomous manner.

MMP production of macrophages is an essential part of pathophysiological mechanisms of COPD (1, 2). To examine the effect of HDAC inactivation, expressions of MMP-2, MMP-9, and MMP-12 were analyzed by RT-PCR. As shown in Fig. 1*E*, these MMPs were up-regulated with the addition of TSA. Based on these results, we hypothesized that the decrease of CD9 and CD81 may be upstream events to the increase of MMPs in macrophages stimulated with cigarette smoke.

mAbs or siRNA Transfection against CD9 and CD81 Enhance MMP Production and Suppress Cell Motility of RAW264.7—To examine if the loss of CD9 and CD81 function is causal to the up-regulation of MMPs, we treated RAW264.7 with function-inhibitory mAbs (13). Co-addition of anti-CD9 mAb, KMC8, and anti-CD81 mAb, 2F7, to RAW264.7 promoted the transcription of MMP-2 and MMP-9, although MMP-12 was unchanged (Fig. 2*A*). Up-regulation of TIMP-1 was also observed; this might be a counteraction against overproduction of MMP-9 (19). In gelatin zymography using culture supernatant, the addition of KMC8 or 2F7 increased gelatinolytic activity of MMP-9 compared with control, and the combination of KMC8 and 2F7 had an additive effect, suggesting a coordinate role of CD9 and CD81 in MMP-9 production (Fig. 2*B*). We failed to detect MMP-2 activity (data not shown) despite its transcription (Fig. 2*A*), possibly because of its defective activation in this cell line (20). MMP-9 activity was also examined by knockdown of CD9 or CD81 with siRNA transfection. As shown in Fig. 2*C*, protein levels of CD9 or CD81 were successfully lowered relative to control, and MMP-9 activity was increased by 75 and 49% in densitometry, respectively.

One of major tetraspanin functions is to regulate cell motility by forming complexes with integrins (21). In fact, we previously demonstrated that CD9 and CD81 complex with β1 and β2 integrins in blood monocytes (13). To study effects of the anti-tetraspanin mAbs on RAW264.7 motility, a migration assay was performed using Transwells (Fig. 2*D*). Although these mAbs did not affect cell proliferation and adhesion (data not shown), KMC8 and 2F7 suppressed migration of RAW264.7 cells on FN. Co-addition of anti-CD9 and anti-CD81 mAbs revealed an additive effect. The migration was dependent on β1 integrins because it was almost completely blocked by anti-integrin β1 mAb. Thus, CD9 and CD81 appeared to regulate integrin-dependent motility as well as MMP production in RAW264.7 macrophages.

CD9/CD81 DKO Mice Spontaneously Develop Pulmonary Emphysema—CD9/CD81 DKO mice were generated in our previous work, which reported that the fusion of mononuclear phagocytes were accelerated in these mice (13). Remarkably, we

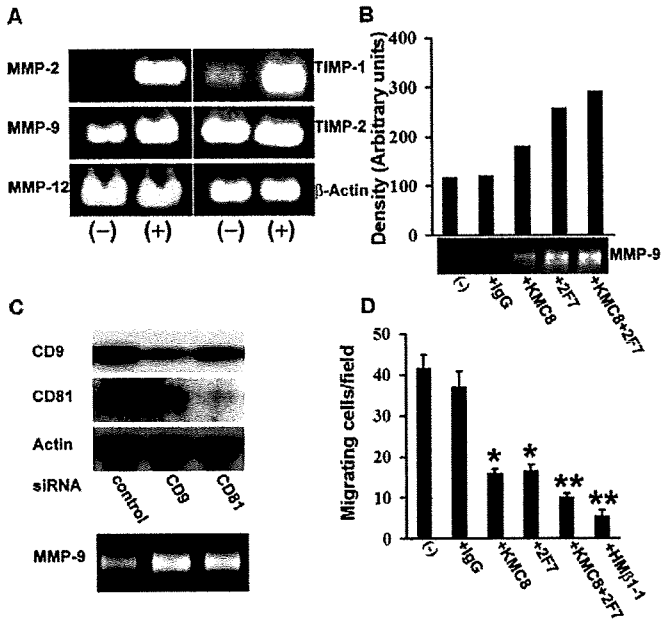

FIGURE 2. **mAbs or siRNA to CD9 and CD81 enhance MMP production and suppress motility of RAW264.7 cells.** *A*, RAW264.7 cells were cultured for 24 h in the absence (−) or presence of KMC8 plus 2F7 (+). mRNA was extracted, and RT-PCR was performed for expressions of MMPs and TIMPs. *B*, RAW264.7 cells were cultured for 24 h in the absence (−) or presence of the indicated mAbs. MMP-9 activity in culture supernatant was examined by gelatin zymography (*lower*) and quantified by densitometry (*upper*). The gelatin zymography is from one representative of three similar experiments. *C*, RAW264.7 was transfected with siRNAs against CD9 or CD81. Decrease in CD9 or CD81 was shown in immunoblotting (*upper*). MMP-9 activity in supernatants of 24-hour culture was examined by gelatin zymography (*lower*). *D*, RAW264.7 cells were applied into the upper chamber of FN-precoated Transwells in the absence (−) or presence of the indicated mAbs. DMEM containing 10% FBS was added to the lower chamber. After 4 h, cells migrating to the lower surface of the membrane were counted after Diff-Quick stain. *Bars* represent the mean ± S.E. *, $p < 0.05$ *versus* IgG; **, $p < 0.05$ *versus* KMC8. *KMC8*, anti-CD9; *2F7*, anti-CD81; *HMβ1-1*, anti-integrin β1.

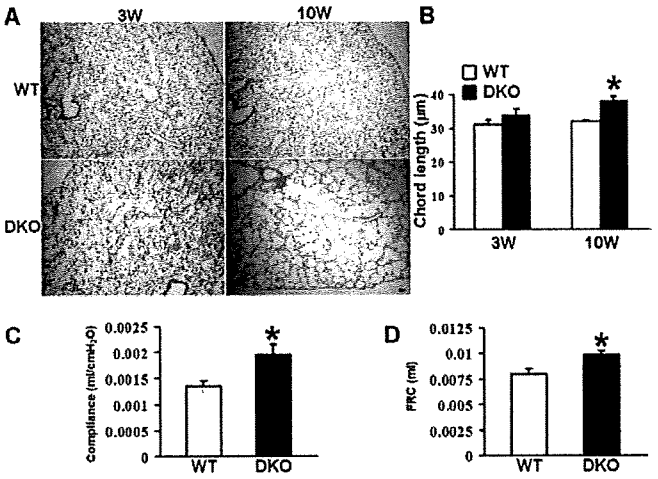

FIGURE 3. **CD9/CD81 DKO mice develop pulmonary emphysema.** *A*, histological lung sections from DKO mice and WT littermates at 3 and 10 weeks of age were stained with hematoxylin and eosin. *Bar*, 50 μm. *B*, chord length measured from the WT and DKO lungs. *C* and *D*, functional tests of the lung. Lung compliance (*C*) and functional residual capacity (*FRC*) (*D*) of mice at 23 weeks of age were measured with a whole body plethysmograph. Values were normalized to body weight. At least three mice were used for each group. *Bars* represent the mean ± S.E. *, $p < 0.05$ *versus* WT.

also found that the DKO mice developed pulmonary emphysema; the mutant lung showed enlargement of airspace and infiltration of inflammatory cells with age (Fig. 3, *A* and *B*, and supplemental Fig. 2). As shown in chord length measurement, the airspace size of CD9/CD81 DKO mice was not different from wild-type (WT) littermates at 3 weeks of age but significantly increased at 10 weeks (Fig. 3*B*). CD9 and CD81 single-KO mice also displayed mild focal airspace enlargement in close examination (supplemental Fig. 2*A*), but their chord lengths at 10 weeks were not significantly different from WT (data not shown). We next assessed the DKO lung using a whole body plethysmograph. When compared with the WT lung, static compliance (Fig. 3*C*) and functional residual capacity (Fig. 3*D*) were significantly increased, indicating physiological impairment of lung function.

It is believed that elastin degradation and remodeling processes occur within human emphysematous lungs (22). To investigate the pathogenesis of the emphysema of DKO lungs in more detail, we did additional staining and ultrastructural studies of histological sections. As shown in Fig. 4, *A* and *B*, elastin fibers appeared to be disrupted, and their network was lost in Elastica-van Gieson stain. Masson's trichrome stain of the enlarged alveolar region revealed abnormal deposition of collagen, suggesting the occurrence of a repair process (Fig. 4, *C* and *D*) (23). Of note, in the terminal bronchiole, Alcian blue/PAS stain detected secretory cell metaplasia of the epithelium (Fig. 4*F*), a finding not present in the WT bronchiole (Fig. 4*E*). In electron microscopy, alveolar macrophages developed many lysosomes and vacuoles (Fig. 4*G*). Some were multinucleated and contained intracytoplasmic needle-shaped inclusions (Fig. 4*H*), which appeared to be phagocytosed collagen as shown previously in destructive process of animal models of emphysema (24). These changes were again not observed in WT macrophages (Fig. 4*I*). There were also abnormal findings in the alveolar septa of the DKO lung. Type II epithelial cells were hypertrophic and contained many lamellar bodies (Fig. 4*J*). Localized increase of elastin and collagen fibers in alveolar walls (Fig. 4*K*), presumably representing structural remodeling (22), was noted when compared with WT (Fig. 4*L*). Collectively, these finding suggest that alveolar destruction and remodeling process were ongoing in the emphysematous lung of DKO mice.

It was previously proposed that apoptosis of septal epithelial and endothelial cells is part of the pathogenesis of emphysema (25). To examine if cell apoptosis contributes to emphysema of the DKO lung, lung sections were stained by terminal deoxynucleotidyltransferase-mediated dUTP nick-end labeling (supplemental Fig. 3*A*), and immunoblotting for active caspase-3 was done using whole lung lysates (supplemental Fig. 3*B*). However, no increase of apoptosis was observed in the DKO lung. We additionally induced apoptosis of bone marrow-derived macrophages (BMDMs) isolated from WT and DKO mice by depriving FBS in culture, but detected no significant difference (supplemental Fig. 3*C*).

Accumulation of Macrophages and Elevation of MMP Activities in the Lung of DKO Mice—Inflammation and protease overactivity are essential causal factors for emphysema lungs in humans (2). To examine if the double deletion of CD9 and CD81 leads to these pathogenic conditions *in vivo*, inflamma-

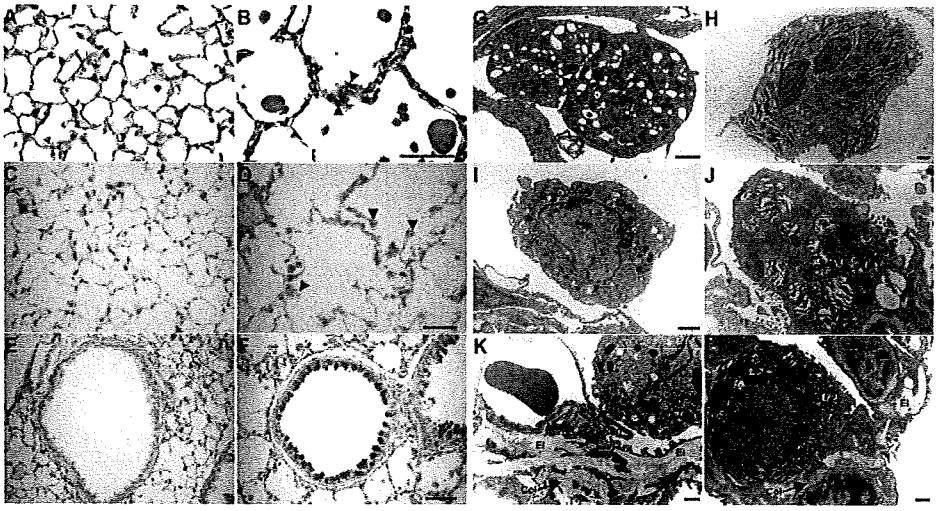

FIGURE 4. **Histological lung sections from DKO mice and WT littermates.** *A–F*, Elastica-van Gieson stain for elastin (*dark blue*) (*A* and *B*), Masson's trichrome stain for collagen (*blue*) (*C* and *D*), and Alcian blue/PAS stain (*E* and *F*) of lung sections from WT (*A*, *C*, and *E*) and DKO (*B*, *D*, and *F*) mice at 10 weeks of age. *Arrowheads* in *B* and *D* indicate sparse elastin fibers and abnormal deposition of collagen, respectively. *Bars*, 50 μm. *G–L*, a macrophage with many lysosomes and vacuoles (*G*), a macrophage containing needle-shaped inclusions (*H*), a hypertrophic type II cells accumulating lamellar bodies (*J*), and increased elastin and collagen fibers (*K*), were shown in electron microscopy of an alveolar region of DKO mice. A macrophage (*I*) and elastin and collagen (*L*) in an alveolar region of a WT littermate were also shown as control. *El*, elastin; *Col*, collagen. *Bars*, 1 μm.

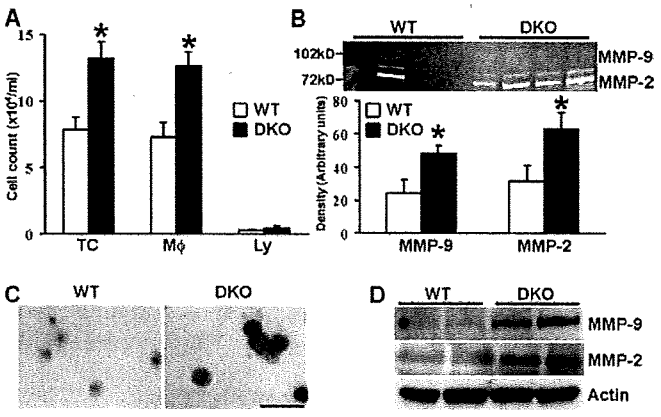

FIGURE 5. **Accumulation of macrophages and elevation of MMP activities in the DKO lung.** *A*, cells isolated from BALF of DKO mice and WT littermates at 10 weeks of age were visualized using Diff-Quick stain, and the number of total cells (*TC*), macrophages (*Mϕ*), and lymphocytes (*Ly*) was determined. *B*, MMP activities in BALF from individuals of DKO mice and WT littermates were examined by gelatin zymography (*upper*) and quantified by densitometry (*lower*). *Bars* represent the mean ± S.E. *, $p < 0.05$ *versus* WT. *C*, macrophages from the BALF were stained with anti-MMP-9 antibody. *Bar*, 100 μm. *D*, expressions of MMP-2 and MMP-9 were examined by immunoblotting using lung homogenate protein from individuals of WT and DKO mice. Anti-actin blots confirm equal amounts of protein loaded in each lane.

tory cells and MMP activities in the DKO lung were evaluated by BALF analysis. As shown in Fig. 5*A*, a larger number of inflammatory cells were isolated from the DKO lung than from WT, and this was because of an increase of macrophages. BALF from CD9 and CD81 single-KO mice contained slightly increased numbers of cells, but they were not significantly different from WT (supplemental Fig. 2*B*). Gelatin zymography showed that the BALF supernatants from DKO mice contained increased proteolytic activities of MMP-2 and MMP-9 (Fig. 5*B*). Also, macrophages isolated from the BALF were strongly stained with anti-MMP-9 antibody especially at the cell periphery, when compared with WT macrophages (Fig. 5*C*). We failed to detect obvious difference in the staining with anti-MMP-2 antibody (data not shown). Increase of the MMP proteins was also confirmed in lysates of the entire lung of DKO mice (Fig. 5*D*).

Macrophages from DKO Mice Are Less Motile and Produce More MMPs than WT—To confirm that motility and MMP production of macrophages in CD9/CD81 DKO mice are intrinsically altered like mAb- or siRNA-treated RAW264.7 cells (Fig. 2), we isolated and cultured BMDMs from DKO mice and compared with WT macrophages *in vitro*. Cell proliferation or cell adhesion onto FN or Matrigel was not different as shown in Fig. 6, *A* and *B*, respectively. However, when migration and random motility were examined in assays using Transwells (Fig. 6*C*) and a time-lapse video microscope (Fig. 6*D* and supplemental video 1), respectively (26), those of DKO macrophages were markedly decreased compared with WT cells. Also, expressions of MMP-2 and MMP-9, but not that of MMP-12, were increased (Fig. 6*E*), similarly to mAb- or siRNA-treated RAW264.7 cells. As a control, we isolated lung fibroblasts from WT and DKO mice and examined MMP-2 and MMP-9 production in gelatin zymography, but we found no differences (data not shown).

Analysis of Gene Expression in CD9/CD81 DKO Macrophages—To gain further information on altered macrophage function of DKO mice, we compared gene expression profiles of BMDMs isolated from WT and DKO mice with oligonucleotide arrays consisting of more than 20,000 mouse genes. The supplemental Tables 1 and 2 list the top 70 genes up-regulated or down-regulated preferentially in the DKO macrophages, respectively. Interestingly, fold differences of the down-regulated genes were higher than those of the up-regulated, also indicating that suppressed genes were much more than induced genes. The induced genes included proteases (carboxypeptidase A5; cathepsin E; cathepsin H; MMP-9; arginyl aminopeptidase (aminopeptidase B)), adhesion-related proteins (cortactin; syndecan 1; glypican 1; integrin αX), and pro-inflammatory cytokine receptors (CD74 (macrophage migration inhibitory factor receptor); colony-stimulating factor 2 receptor). Meanwhile, the suppressed genes included an antioxidant protein (ceruloplasmin), a protease inhibitor (serine peptidase inhibitor, clade B, members 5 (Maspin)), and extracellular matrix proteins (integrin-binding sialoprotein; secreted acidic cysteine-rich glycoprotein (osteonectin); biglycan; matrilin 3). It is of note that fucosyltransferase 8 was listed as a down-regulated gene in the DKO macrophages, because the deficiency of this glycosyltransferase was recently reported to impair $\alpha 3\beta 1$ inte-

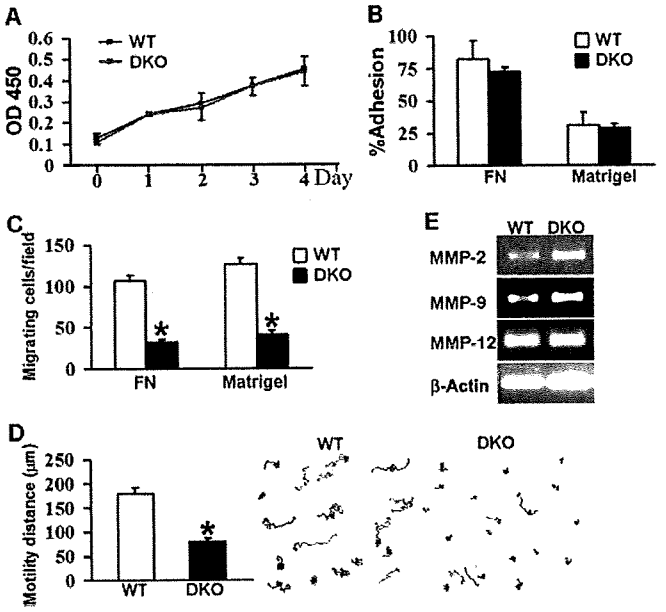

FIGURE 6. **BMDMs from DKO mice are less motile and produce more MMPs than WT.** *A*, BMDMs from DKO mice or WT littermates at 10 weeks of age were cultured in DMEM containing 20% FBS and 30% L929 supernatant. Cell proliferation was quantified using Cell Counting Kit-8. *B*, BMDMs in serum-free DMEM were cultured on FN- or Matrigel-precoated wells for 1.5 h. After unattached cells were removed, adherent cells were quantified with Cell Counting Kit-8. *C*, BMDMs in serum-free DMEM were applied to the upper chamber of Transwells that were precoated with FN or Matrigel. DMEM containing 10% FBS was added to the lower chamber. After 4 h, cells migrating to the lower surface were counted with Diff-Quick stain. *D*, BMDMs were plated onto Matrigel-precoated dishes. Images were acquired every minute for 90 min, and tracks (*right*) and distances (*left*) of random motility were determined using Scion Image tools. Values represent the mean ± S.E. *, $p < 0.05$ *versus* WT. *E*, mRNA was extracted from BMDMs, and expressions of MMP-2, MMP-9, and MMP-12 were analyzed by RT-PCR. β-Actin amplification was internal control.

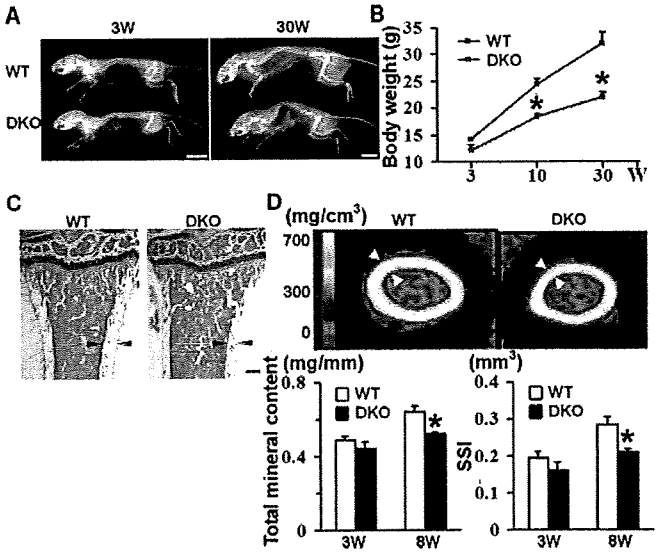

FIGURE 7. **CD9/CD81 DKO mice display body weight loss, kyphosis, and osteopenia.** *A*, whole body radiographs of WT and DKO mice at 3 and 30 weeks of age. *Bars*, 10 mm. *B*, time course of body weight of WT and DKO littermates. *C*, toluidine blue stain of longitudinal sections of proximal tibia at 8 weeks of age. Note that cortical bone of the DKO mouse is thinner than that of the WT littermate (*arrowheads*). *Bar*, 250 μm. *D*, pQCT images of femoral diaphysis at 8 weeks of age (*upper*). Mineral densities are shown as different colors according to the standard mineral density gradients. Note the reduction in cortical thickness of the DKO mouse (*arrowheads*). Total mineral content and strength strain index (*SSI*) were also determined (*lower*). Trabecular parameters were not different between WT and DKO mice (data not shown). Values represent the mean ± S.E. *, $p < 0.05$ *versus* WT.

grin-mediated cell migration and cause pulmonary emphysema in mice (27). Expressions of other tetraspanins, including CD37, CD53, CD82, and CD151, were unremarkably changed (data not shown).

CD9/CD81 DKO Mice Also Display Body Weight Loss, Kyphosis, and Osteopenia—With aging, the DKO mice could be discriminated from WT (Fig. 7*A*) and CD9 or CD81 single-KO littermates (data not shown) by progressive kyphotic appearance, as shown in whole body radiographs. Moreover, weight loss became evident over time when compared with WT mice (Fig. 7*B*). Histological sections of proximal tibia displayed that, although the trabecular bone appeared normal, the cortical bone of DKO mice was thinner than WT (Fig. 7*C*). Images of femoral diaphysis in pQCT analysis also showed a decrease in cortical bone thickness and age-dependent reduction in total mineral content and strength strain index (Fig. 7*D*). Decrease in these parameters was not observed in CD9 or CD81 single-KO mice (data not shown). To investigate the pathophysiology of the osteopenic phenotype in more detail, histomorphometric analysis was done with the proximal tibia of DKO mice (supplemental Fig. 4). Consistently with the histological appearance of the trabecular bone (Fig. 7*C*), there were no significant differences in trabecular bone volume and trabecular thickness (supplemental Fig. 4*A*). The number of osteoclasts in the DKO mice was increased by 60% when compared with WT (supplemental Fig. 4*B*). This seems to reflect elevated fusogenic capacity of DKO macrophages *in vitro* (supplemental Fig. 4*C*) and is consistent with our previous observation (13). However, eroded surface was decreased (supplemental Fig. 4*B*), suggesting that osteoclast activity was unexpectedly impaired. Meanwhile, osteoblast activity was likewise reduced. The number of osteoblasts and the surface of osteoblasts were decreased, and their function in matrix production was damaged as indicated by the decreased thickness of newly deposited matrix (osteoid thickness) (supplemental Fig. 4, *D* and *E*). To perform kinetic analysis of bone formation and mineralization, mice were intraperitoneally injected twice with calcein at a 3-day interval. Compared with WT, the distance of two labeled bands was shorter in the DKO mice (supplemental Fig. 4*F*), resulting in decreased mineral apposition rate and bone formation rate in trabecular dynamic histomorphometry (supplemental Fig. 4*G*). These results indicate that, although osteoclastogenesis is accelerated, both osteolytic and osteoblastic activities were impaired and that the decrease of bone formation rather exceeded that of bone resorption.

We further analyzed histological sections of muscle, skin, eye, heart, aorta, liver, and kidney, but no obvious difference was observed between WT and DKO mice. Hemoglobin and the number of leukocytes and platelets determined in peripheral blood analysis were normal. Serum levels of total protein, albumin, cholesterol, triglyceride, calcium, and creatinine were also not different (data not shown). Thus, the phenotype is unlikely to be caused by malnutrition, and the CD9/CD81 DKO

mouse is not a premature aging model such as *klotho* mice, which exhibits ectopic calcifications, arteriosclerosis, skin atrophy, and cardiac dysfunction in addition to pulmonary emphysema and osteopenia (28).

DISCUSSION

At specialized membrane microdomains, tetraspanins facilitate the formation of multimolecular complexes and regulate cell morphology, motility, invasion, fusion, and signaling. Based on these characteristics, they are also referred to as molecular facilitator or organizer (6). Tetraspanins have been extensively studied in cancer biology. They affect tumor cell motility *in vitro* and tumor metastasis *in vivo* most likely by regulating function of integrins and production of MMPs (7–9, 29). However, it has not been investigated if tetraspanins play a role in motility and MMP production of macrophages. Using a mAb- or siRNA-treated macrophage line, RAW264.7 (Fig. 2), and primary DKO macrophages (Fig. 6), we have shown that dysfunction of CD9 and CD81 suppresses cell motility and promoted the production of MMP-2 and MMP-9 *in vitro*. CD9/CD81 double deletion also caused increase of macrophages and elevation of MMP-2 and MMP-9 activities in the mouse lung *in vivo* (Fig. 5). Thus, co-deficiency of CD9 and CD81 function seems to be sufficient for macrophages to increase MMP production as well as to suppress cell motility. Suppressed motility of macrophages does not necessarily contradict with their infiltration into the lung. For example, macrophages from SH2-containing inositol-5-phosphatase 1 (SHIP1) KO mice, which revealed massive infiltration of macrophages in alveolar air spaces, exhibited defects in motility *in vitro* (30). In these mice, decreased efflux of macrophages from the airspace, rather than their increased influx into the airspace, might contribute to macrophage accumulation. The expression of MMPs is regulated by multiple factors, including growth factors and their receptors, cell adhesion molecules, and GTPases (31). We speculate that CD9 and CD81 coordinately assemble these factors in their own microdomains and thereby indirectly control the production of MMPs (6).

Expression of inflammatory genes is determined by a balance between histone acetylation, which activates transcription, and deacetylation, which switches off transcription. In humans, cigarette smoke suppresses the activity of HDAC in alveolar macrophages, and this was correlated with increased expression of inflammatory genes, including TNF-α and IL-8 in these cells. There was also a reduction in HDAC activity in peripheral lung and alveolar macrophages from COPD patients, and this was correlated with disease severity (5). We cultured RAW264.7 cells in the presence of CSE, the HDAC inhibitor TSA, and pro-inflammatory cytokines IFN-γ and TNF-α, and all these treatments but TNF-α down-regulated the protein levels of both CD9 and CD81 (Fig. 1 and supplemental Fig. 1). These results raise an hypothesis that cigarette smoke reduces the HDAC activity, switching on inflammatory genes and leading to the down-regulation of CD9 and CD81 in macrophages. The resultant insufficiency of CD9 and CD81 functions may be part of important mechanisms that cause or exacerbate the accumulation of alveolar macrophages and their overproduction of MMPs in cigarette smokers.

CD9 single-KO mice are infertile because of impaired oocyte fusion with sperm (32). CD81 single-KO mice show likewise impaired oocyte fertilization (33) in addition to altered immune response (34, 35). KO mice of single tetraspanin have so far resulted in relatively mild phenotype. One possible reason is that the loss of a single tetraspanin may be compensated by other tetraspanins (21). In this study, double deletion of CD9 and CD81 in mice leads to the lung phenotype morphologically and functionally mimicking the emphysematous lung in human COPD (Fig. 3). The CD9/CD81 DKO mice displayed age-dependent progression of airspace enlargement. Secretory cell metaplasia, a finding similar to goblet cell metaplasia in cigarette smokers (36), was also observed. It is unlikely that the emphysema resulted from defective alveolization, because mouse alveolization is completed by 3 weeks (37). Moreover, the elastin/collagen staining and ultrastructural studies of histological sections suggested that alveolar destruction and remodeling process were ongoing in the DKO lung (Fig. 4). Thus, together with the findings of macrophage infiltration and elevated MMP activities in the lung (Fig. 5), it appears that inflammatory and elastolytic processes caused emphysema in the DKO mice. In the gene expression profile of DKO macrophages, multiple proteases, including MMP-9, were induced (supplemental Table 1), whereas the antioxidant protein ceruloplasmin, the protease inhibitor Maspin, and multiple extracellular matrix proteins were suppressed (supplemental Table 2). Although these differential gene expressions remain to be validated with quantitative PCR, the profile was consistent with the hypothesis that the imbalances of proteases/antiproteases and oxidants/antioxidants were present in the DKO macrophages as proposed previously for molecular mechanisms in macrophages orchestrating the progression of emphysema (2).

Common extrapulmonary effects of COPD include weight loss and osteoporosis, mechanisms of which have been poorly understood (38, 39). Interestingly, the CD9/CD81 DKO mice displayed age-dependent weight loss and osteopenia (Fig. 7). The number of osteoclasts was increased because of the enhanced fusion of their progenitors of the macrophage lineage, but the osteopenia was caused not by increased bone resorption but by decreased bone formation (supplemental Fig. 4), indicating low turnover osteopenia. This type of osteopenia occurs as an aging process in humans (40), and it has been proposed that there are clear parallels between the pathophysiological responses to aging and those involved in COPD (41). To assess the function of the DKO osteoblasts *in vitro*, we isolated and cultured bone marrow cells in the presence of ascorbic acid and β-glycerophosphate and stained mineralized nodules with alizarin red (42). However, preliminary results failed to reveal obvious differences between WT and DKO mice (data not shown). Possibly, the impaired bone formation in DKO mice might be attributed not to primary defects of osteoblasts but to their microenvironmental factors such as hormones, cytokines, growth factors, MMPs, and extracellular matrix proteins